2

Gearbox Simulation Models with Gear and Bearing Faults

Endo Hiroaki[1] and Sawalhi Nader[2]
[1]*Test Devices Inc.,*
[2]*Prince Mohammad Bin Fahd University (PMU),*
Mechanical Engineering Department, AlKhobar
[1]*USA*
[2]*Saudi Arabi*

1. Introduction

Simulation is an effective tool for understanding the complex interaction of transmission components in dynamic environment. Vibro-dynamics simulation of faulty gears and rolling element bearings allows the analyst to study the effect of damaged components in controlled manners and gather the data without bearing the cost of actual failures or the expenses associated with an experiment that requires a large number of seeded fault specimens. The fault simulation can be used to provide the data required in training Neural network based diagnostic/prognostic processes.

2. Key elements in gearbox simulation

2.1 Transmission error

Gears, by their inherent nature, cause vibrations due to the large pressure which occurs between the meshing teeth when gears transmit power. Meshing of gears involves changes in the magnitude, the position and the direction of large concentrated loads acting on the contacting gear teeth, which as a result causes vibrations. Extended period of exposure to noise and vibration are the common causes of operational fatigue, communication difficulties and health hazards. Reduction in noise and vibration of operating machines has been an important concern for safer and more efficient machine operations.

Design and development of quieter, more reliable and more efficient gears have been a popular research area for decades in the automotive and aerospace industries. Vibration of gears, which directly relates to noise and vibration of the geared machines, is typically dominated by the effects of the tooth meshing and shaft revolution frequencies, their harmonics and sidebands, caused by low (shaft) frequency modulation of the higher tooth-mesh frequency components. Typically, the contribution from the gear meshing components dominates the overall contents of the measured gearbox vibration spectrum (see Figure-2.1.1).

Transmission Error (TE) is one of the most important and fundamental concepts that forms the basis of understanding vibrations in gears. The name 'Transmission Error' was originally coined by Professor S. L. Harris from Lancaster University, UK and R.G. Munro,

his PhD student at the time. They came to the realization that the excitation forces causing the gears to vibrate were dependent on the tooth meshing errors caused by manufacturing and the bending of the teeth under load [1].

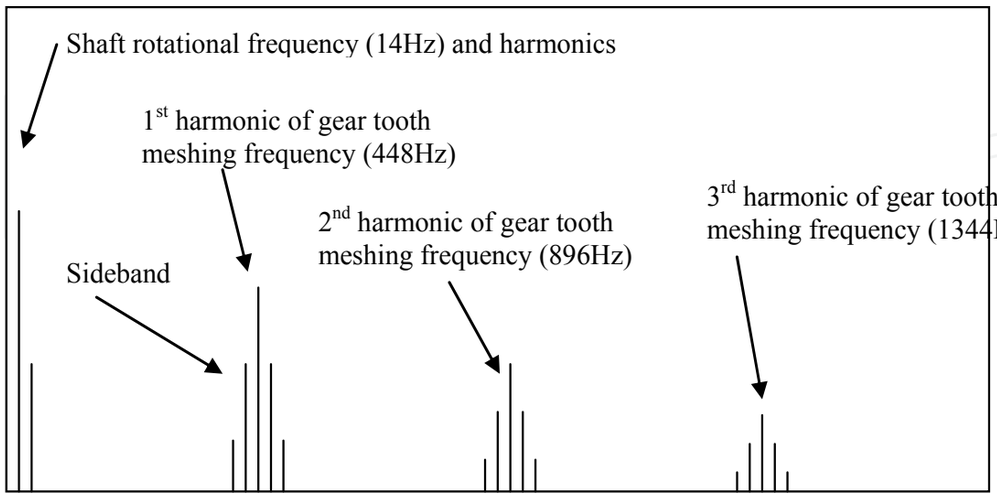

(Number of Teeth = 32)

Fig. 2.1.1. Typical spectrum composition of gear vibration signal.

TE is defined as the deviation of the angular position of the driven gear from its theoretical position calculated from the gearing ratio and the angular position of the pinion (Equation-2.1.1). The concept of TE is illustrated in Figure-2.1.2.

$$TE = \left(\theta_{gear} - \frac{R_{pinion}}{R_{gear}} \theta_{pinion} \right) \tag{2.1.1}$$

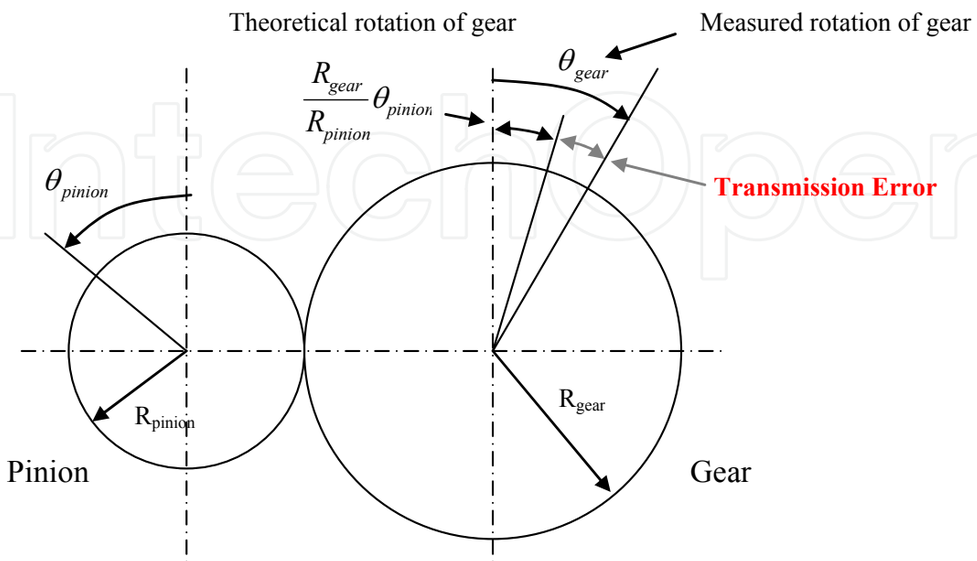

Fig. 2.1.2. Definition of Transmission Error.

What made the TE so interesting for gear engineers and researchers was its strong correlation to the gear noise and the vibrations. TE can be measured by different types of instruments. Some commonly used methods are: Magnetic signal methods, straingauge on the drive shaft, torsional vibration transducers, tachometers, tangential accelerometers and rotary encoders systems. According to Smith [2], TE results from three main sources: 1) Gear geometrical errors, 2) Elastic deformation of the gears and associated components and 3) Errors in mounting. Figure-2.1.3 illustrates the relationship between TE and its sources.

Transmission Error exists in three forms: 1) Geometric, 2) Static and 3) Dynamic. Geometric TE (GTE) is measured at low speeds and in the unloaded state. It is often used to examine the effect of manufacturing errors. Static TE (STE) is also measured under low speed conditions, but in a loaded state. STE includes the effect of elastic deflection of the gears as well as the geometrical errors. Dynamic TE (DTE) includes the effects of inertia on top of all the effects of the errors considered in GTE and in STE. The understanding of the TE and the behaviour of the machine elements in the geared transmission system leads to the development of realistic gear rotor dynamics models.

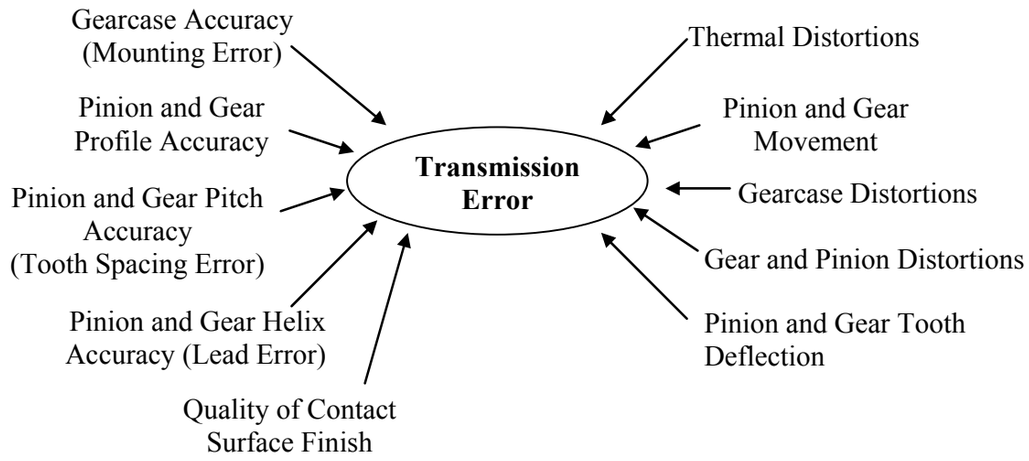

Fig. 2.1.3. Sources of Transmission Error.

2.2 Effect of gear geometric error on transmission error

A typical GTE of a spur gear is shown in Figure-2.2.1. It shows a long periodic wave (gear shaft rotation) and short regular waves occurring at tooth-mesh frequency. The long wave is often known as: Long Term Component: LTC, while the short waves are known as: Short Term Component: STC.

The LTC is typically caused by the eccentricity of the gear about its rotational centre. An example is given in Figure-2.2.2 to illustrate how these eccentricities can be introduced into the gears by manufacturing errors; it shows the error due to a result of the difference between the hobbing and the shaving centres.

The effect of errors associated with gear teeth appears in the STC as a localized event. The parabolic-curve-like effect of tooth tip relief is shown in Figure-2.2.3(a). The STC is caused mainly by gear tooth profile errors and base pitch spacing error between the teeth. The effect

of individual tooth profile errors on the GTE is illustrated in Figure-2.2.3(a). The GTE of a meshing tooth pair is obtained by adding their individual profile errors. The STC of gear GTE is synthesised by superposing the tooth pair GTEs separated by tooth base pitch angles (Figure-2.2.3 (b)).

Another common gear geometric error is tooth spacing or pitch errors, shown in Figure-2.2.4. The tooth spacing error appears in GTE as vertical raise or fall in the magnitude of a tooth profile error.

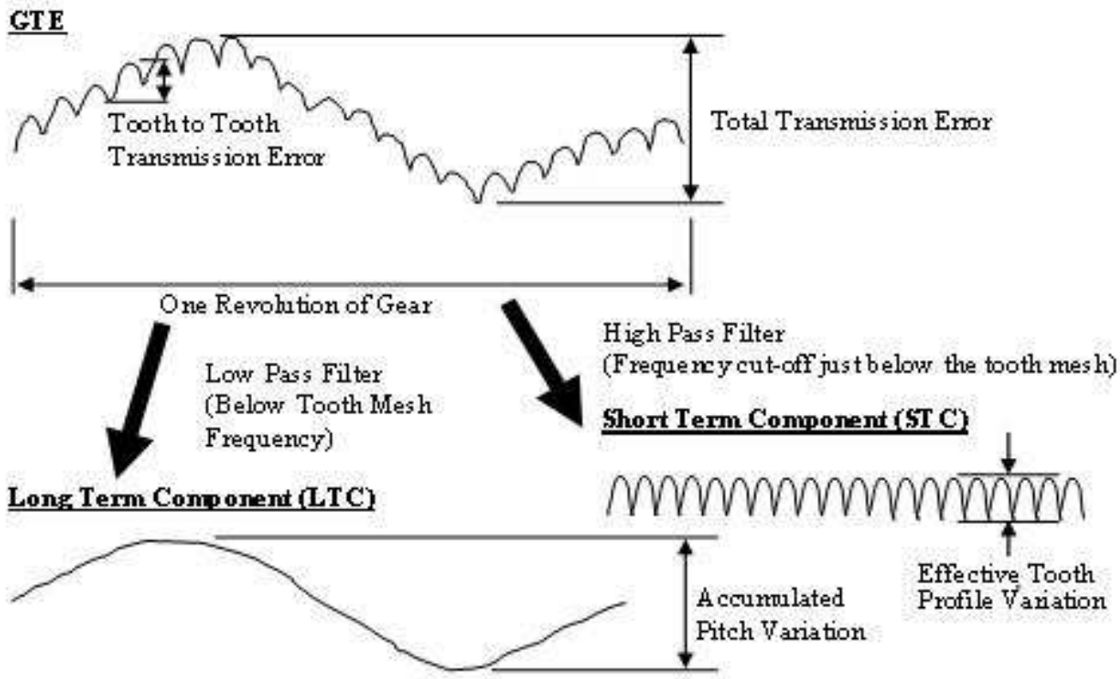

Fig. 2.2.1. A typical Geometrical Transmission Error.

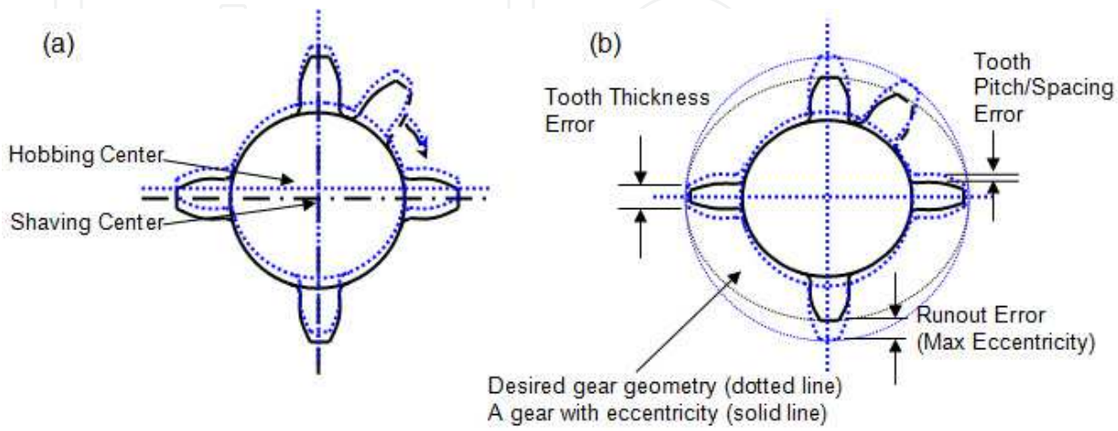

Fig. 2.2.2. (a) Eccentricity in a gear caused by manufacturing errors, (b) Resulting errors in gear geometry.

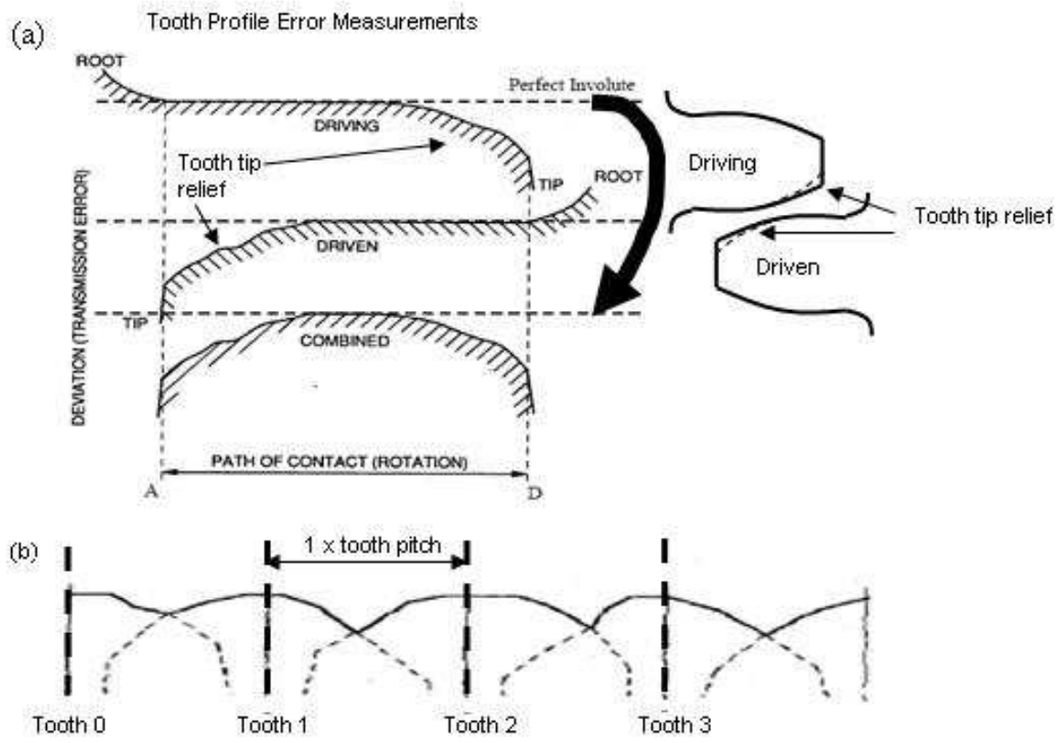

Fig. 2.2.3. (a) GTE of a meshing tooth pair (b) Resulting Short Term Component of GTE.

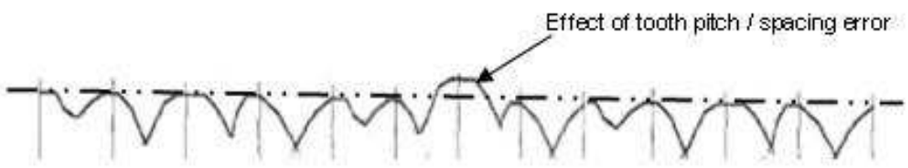

Fig. 2.2.4. Effect of spacing error appearing in short term component of GTE.

2.3 Effect of load on transmission error

Elastic deflections occurring in gears are another cause of TE. Although gears are usually stiff and designed to carry very large loads, their deflection under load is not negligible. Typical deflection of gear teeth occurs in the order of microns (μm). Although it depends on the amount of load gears carry, the effect of the deflection on TE may become more significant than the contribution from the gear geometry.

A useful load-deflection measure is that 14N of load per 1mm of tooth face width results in 1μm of deflection for a steel gear: i.e. stiffness = $14E10^9$ N/m/m for a tooth pair meshing at the pitch line. It is interesting to note here that the stiffness of a tooth pair is independent of its size (or tooth module) [3]. Deflection of gear teeth moves the gear teeth from their theoretical positions and in effect results in a continuous tooth pitch error: see Figure-2.3.1 (a). The effect of the gear deflection appears in the TE (STE) as a shifting of the GTE: Figure-2.3.1 (b).

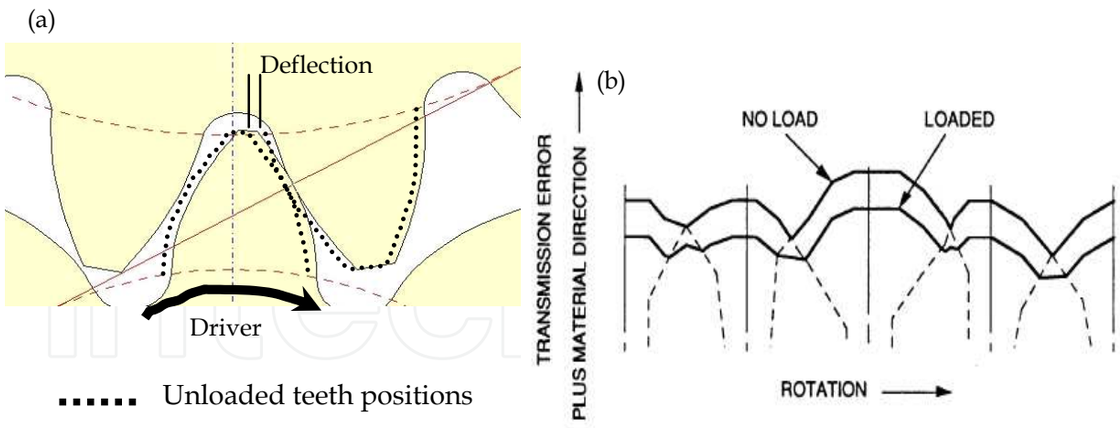

Fig. 2.3.1. (a) Deflection of gear tooth pair under load, (b) Effect of load on transmission error (TE).

Consider the more general situation where the deflection in loaded gears affects the TE significantly. Note that the following discussion uses typical spur gears (contact ratio = 1.5) with little profile modification to illustrate the effect of load on TE. Figure-2.3.2 illustrates the STE caused by the deflection of meshing gear teeth. The tooth profile chart shows a flat

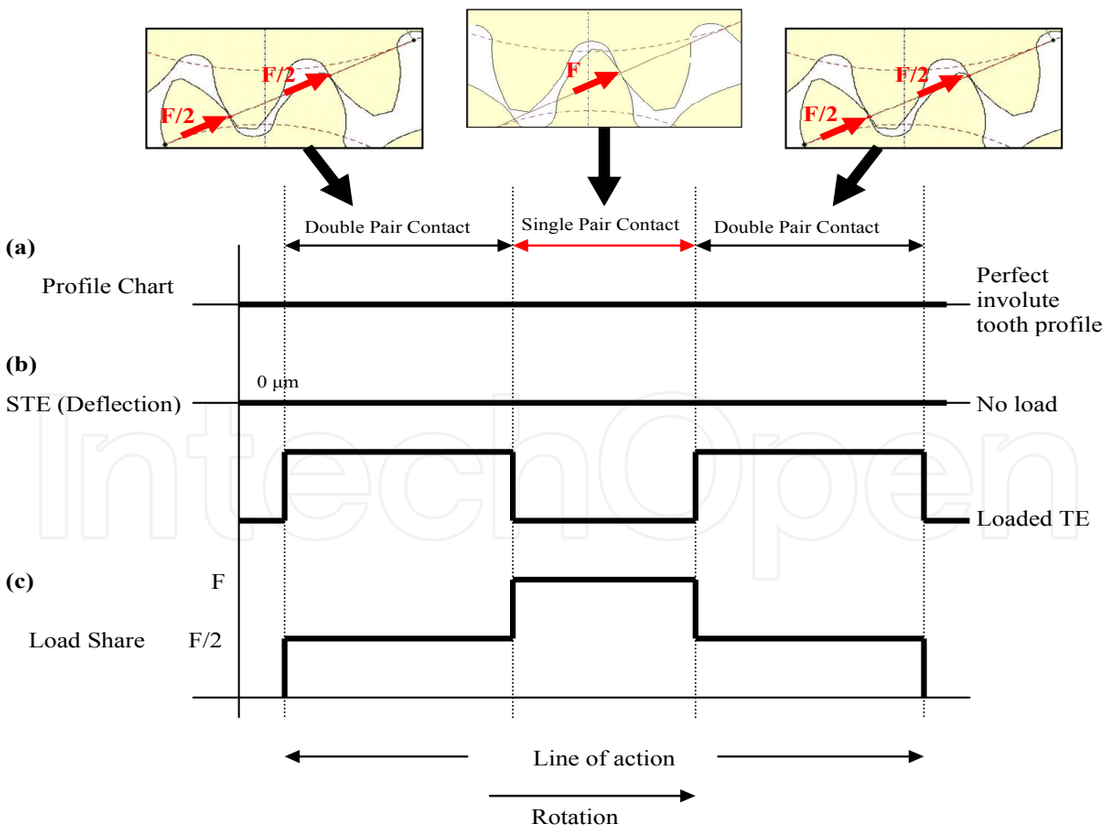

Fig. 2.3.2. Effect of Load on TE, (a) Tooth Profile Chart, (b) Static Transmission Error, (c) Loading acting on a tooth

line indicating the ideal involute profile of the tooth: Figure-2.3.2 (a). The effect of mesh stiffness variation due to the change in the number of meshing tooth pairs appears as steps in the STE plot: Figure-2.3.2 (b). The amount of deflection increases when a single pair of teeth is carrying load and decreases when the load is shared by another pair. The share of force carried by a tooth through the meshing cycle is shown in Figure-2.3.2 (c).

A paper published jointly by S.L. Harris, R. Wylie Gregory and R.G. Munro in 1963 showed how transmission error can be reduced by applying appropriate correction to the involute gear profile [4, 5]. The Harris map in Figure-2.3.3 shows that any gear can be designed to have STE with zero variation (i.e. a flat STE with constant offset value) for a particular load. The basic idea behind this technique is that the profile of gear teeth can be designed to cancel the effect of tooth deflection occurring at the given load.

Additionally, variation of TE can be reduced by increasing the contact ratio of the gear pair. In other words, design the gears so that the load is carried by a greater number of tooth pairs.

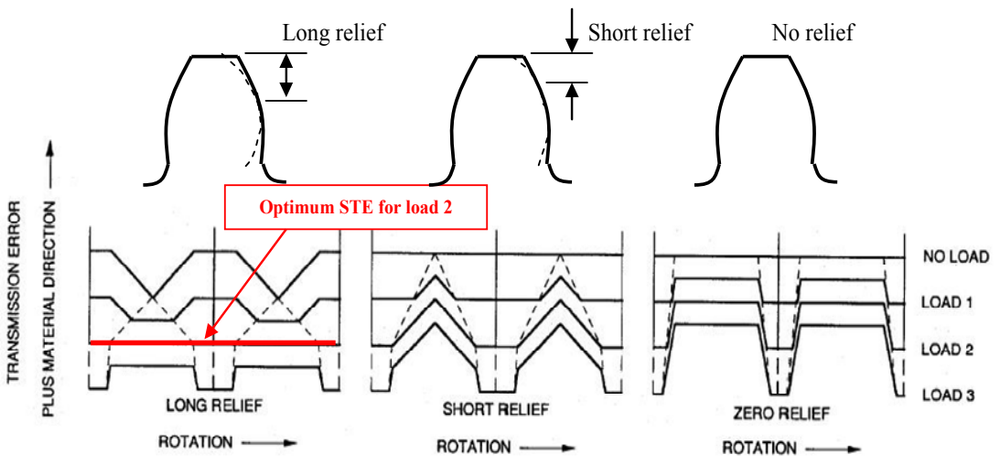

Fig. 2.3.3. Optimum tooth profile modification of a spur gear.

2.4 Modelling gear dynamics

It is a standardized design procedure to perform STE analysis to ensure smoothly meshing gears in the loaded condition. It was explained in this section how the strong correlation between the TE and the gear vibration makes the TE a useful parameter to predict the quietness of the gear drives. However, a more realistic picture of the gear's dynamic properties can not be captured without modelling the dynamics of the assembled gear drive system. Solution of engineering problems often requires mathematical modelling of a physical system. A well validated model facilitates a better understanding of the problem and provides useful information for engineers to make intelligent and well informed decisions.

A comprehensive summary of the history of gear dynamic model development is given by Ozguven and Houser [6]. They have reviewed 188 items of literature related to gear dynamic simulation existing up to 1988. In Table-2.4.1, different types of gear dynamics models were classified into five groups according to their objectives and

Group-1: Simple Dynamic Factor Models Most early models belong to this group. The model was used to study gear dynamic load and to determine the value of dynamic factor that can be used in gear root stress formulae. Empirical, semi-empirical models and dynamic models constructed specifically for determination of dynamic factor are included in this group.
Group-2: Models with Tooth Compliance Models that consider tooth stiffness as the only potential energy storing element in the system. Flexibility of shafts, bearings etc is neglected. Typically, these models are single DOF spring-mass systems. Some of the models from this group are classified in group-1 if they are designed solely for determining the dynamic factor.
Group-3: Models for Gear Dynamics A model that considers tooth compliance and the flexibility of the relevant components. Typically these models include torsional flexibility of shafts and lateral flexibility of bearings and shafts along the line of action.
Group-4: Models for Geared Rotor Dynamics This group of models consider transverse vibrations of gear carrying shafts as well as the lateral component *(NOTE: Transverse: along the Plane of Action, Lateral: Normal to the Plane of Action).* Movement of the gears is considered in two mutually perpendicular directions to simulate, for example, whirling.
Group-5: Models for Torsional Vibrations The models in the third and fourth groups consider the flexibility of the gear teeth by including a constant or time varying mesh stiffness. The models belonging to this group differentiate themselves from the third and fourth groups by having rigid gears mounted on flexible shafts. The flexibility at the gearmesh is neglected. These models are used in studying pure (low frequency) torsional vibration problems.

Table 2.4.1. Classification of Gear Dynamic Models. (Ozguven & Houser [6])

functionality. Traditionally lumped parameter modelling (LPM) has been a common technique that has been used to study the dynamics of gears. Wang [7] introduced a simple LPM to rationalize the dynamic factor calculation by the laws of mechanics. He proposed a model that relates the GTE and the resulting dynamic loading. A large number of gear dynamic models that are being used widely today are based on this work. The result of an additional literature survey on more recently published materials by Bartelmus [8], Lin & Parker [9, 10], Gao & Randall [11, 12], Amabili & Rivola [13], Howard et al [14], Velex & Maatar [15], Blankenship & Singh [17], Kahraman & Blankenship [18] show that the fundamentals of the modelling technique in gear simulations have not changed and the LMP method still serves as an efficient technique to model the wide range of gear dynamics behaviour. More advanced LPM models incorporate extra functions to simulate specialized phenomena. For example, the model presented by P. Velex and M. Maatar [15] uses the individual gear tooth profiles as input and calculates the GTE directly from the gear tooth profile. Using this method they simulated how the change in contact behaviour of meshing gears due to misalignment affects the resulting TE.

FEA has become one of the most powerful simulation techniques applied to broad range of modern Engineering practices today. There have been several groups of researchers who attempted to develop detailed FEA based gear models, but they were troubled by the

challenges in efficiently modelling the rolling Hertzian contact on the meshing surfaces of gear teeth. Hertzian contact occurs between the meshing gear teeth which causes large concentrated forces to act in very small area. It requires very fine FE mesh to accurately model this load distribution over the contact area. In a conventional finite element method, a fully representative dynamic model of a gear requires this fine mesh over each gear tooth flank and this makes the size of the FE model prohibitively large.

Researchers from Ohio State University have developed an efficient method to overcome the Hertzian contact problem in the 1990s' [16]. They proposed an elegant solution by modelling the contact by an analytical technique and relating the resulting force distribution to a coarsely meshed FE model. This technique has proven so efficient that they were capable of simulating the dynamics of spur and planetary gears by [19, 20] (see Figure-2.4.1). For more details see the CALYX user's manuals [21, 22].

For the purpose of studies, which require a holistic understanding of gear dynamics, a lumped parameter type model appears to provide the most accessible and computationally economical means to conduct simulation studies.

A simple single stage gear model is used to explain the basic concept of gear dynamic simulation techniques used in this chapter. A symbolic representation of a single stage gear system is illustrated in Figure-2.4.2. A pair of meshing gears is modelled by rigid disks representing their mass/moment of inertia. The discs are linked by line elements that represent the stiffness and the damping (representing the combined effect of friction and fluid film damping) of the gear mesh. Each gear has three translational degrees of freedom (one in a direction parallel to the gear's line of action, defining all interaction between the gears) and three rotational degree of freedoms (DOFs). The stiffness elements attached to the centre of the disks represent the effect of gear shafts and supporting mounts. NOTE: Symbols for the torsional stiffnesses are not shown to avoid congestion.

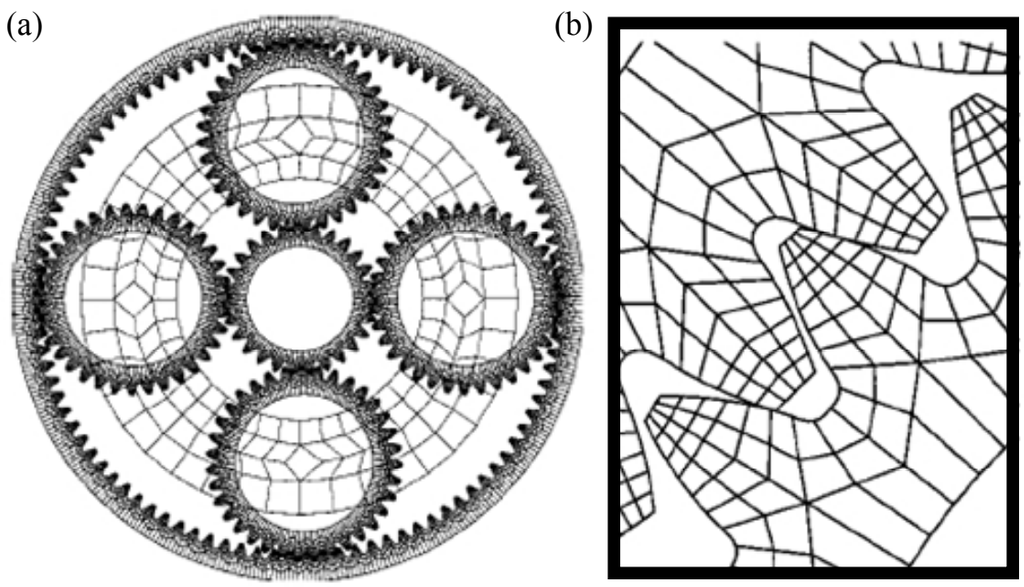

Fig. 2.4.1. (a) Parker's planetary gear model and (b) FE mesh of gear tooth. Contacts at the meshing teeth are treated analytically. It does not require dense FE mesh.
(Courtesy of Parker et al. [20])

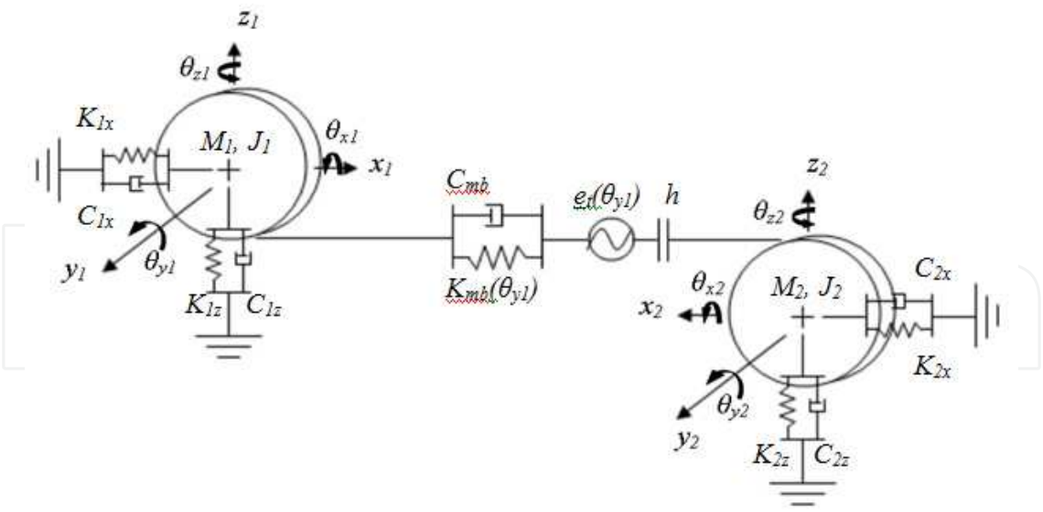

x_i, y_i, z_i Translation at i_{th} Degrees of Freedom.

$\theta_{xi}, \theta_{yi}, \theta_{zi}$ Rotation about a translational axis at i_{th} Degrees of Freedom.

C, C_{mb} Damping matrices. The subscript '*mb*' refers to damping at the gearmesh. Typically for C_{mb}, $\zeta = 3 \sim 7\%$.

K, K_{mb} Linear stiffness elements. The subscript '*mb*' refers to stiffness at the gearmesh.

h An 'on/off' switch governing the contact state of the meshing gear teeth.

$\underline{e_t}$ A vector representing the combined effect of tooth topography deviations and misalignment of the gear pair.

i Index: i=1,2, 3 …etc.

Fig. 2.4.2. A Typical Lumped Parameter Model of Meshing Gears.

The linear spring elements representing the Rolling Element Bearings (REB) are a reasonable simplification of the system that is well documented in many papers on gear simulation. For the purpose of explaining the core elements of the gear simulation model, the detail of REB as well as the casing was omitted from this section; more comprehensive model of a gearbox, with REB and casing, will be presented later in section 2.5.

Vibration of the gears is simulated in the model as a system responding to the excitation caused by a varying TE, 'e_t' and mesh stiffness 'K_{mb}'. The dominant force exciting the gears is assumed to act in a direction along the plane of action (PoA). The angular position dependent variables 'e_t' and 'K_{mb}' are expressed as functions of the pinion pitch angle (θ_{y1}) and their values are estimated by using static simulation. Examples of similar techniques are given by Gao & Randall [11, 12], Du [23] and Endo and Randall [61].

Equations of motion derived from the LPM are written in matrix format as shown in Equation-2.4.1. The equation is rearranged to the form shown in the Euqation-2.4.2; the effect of TE is expressed as a time varying excitation in the equation source. The dynamic response of the system is simulated by numerically solving the second order term (accelerations) for each step of incremented time. The effect of the mesh stiffness variation is implemented in the model by updating its value for each time increment.

$$M\ddot{\underline{x}} + C\left(\dot{\underline{x}} - \dot{\underline{e}}_t\right) + K\left(\underline{x} - \underline{e}_t(\theta)\right) = F_s \tag{2.4.1}$$

$$M\ddot{\underline{x}} + C\dot{\underline{x}} + K\underline{x} = F_s + hC_{mb}(\theta)\dot{\underline{e}}_t + hK_{mb}(\theta)\underline{e}_t \tag{2.4.2}$$

where,

$\underline{x}$, $\dot{\underline{x}}$, $\ddot{\underline{x}}$ Vectors of translational and rotational displacement, velocity and acceleration.

θ Angular position of pinion.

K, K_{mb} Stiffness matrices (where K includes the contribution from K_{mb}). The subscript '*mb*' refers to stiffness at the gearmesh.

C, C_{mb} Damping matrices (C including contribution from C_{mb}). The subscript '*mb*' refers to damping at the gearmesh.

h An 'on/off' switch governing the contact state of the meshing gear teeth.

F Static force vector.

$\underline{e}_t$, $\dot{\underline{e}}_t$ A vector representing the combined effect of tooth topography deviations.

2.5 Modelling rolling element bearings and gearbox casing

For many practical purposes, simplified models of gear shaft supports (for example, the effect of rolling element bearings (REBs) and casing were modelled as simple springs with constant stiffnesses) can be effective tools. However, fuller representations of these components become essential in the pursuit of more complete and accurate simulation modelling.

For a complete and more realistic modelling of the gearbox system, detailed representations of the REBs and the gearbox casing are necessary to capture the interaction amongst the gears, the REBs and the effects of transfer path and dynamics response of the casing.

Understanding the interaction between the supporting structure and the rotating components of a transmission system has been one of the most challenging areas of designing more detailed gearbox simulation models. The property of the structure supporting REBs and a shaft has significant influence on the dynamic response of the system. Fuller representation of the REBs and gearbox casing also improves the accuracy of the effect transmission path that contorts the diagnostic information originated from the faults in gears and REBs. It is desired in many applications of machine health monitoring that the method is minimally intrusive on the machine operation. This requirement often drives the sensors and/or the transducers to be placed in an easily accessible location on the machine, such as exposed surface of gearbox casing or on the machine skid or on an exposed and readily accessible structural frame which the machine is mounted on.

The capability to accurately model and simulate the effect of transmission path allows more realistic and effective means to train the diagnostic algorithms based on the artificial intelligence.

2.5.1 Modelling rolling element bearings

A number of models of REBs exist in literatures [24, 25, 26, 27] and are widely employed to study the dynamics and the effect of faults in REBs. The authors have adopted the 2 DoF model originally developed by Fukata [27] in to the LPM of the gearbox. Figure-2.5.1 (a)

illustrates the main components of the rolling element bearing model and shows the load zone associated with the distribution of radial loads in the REB as it supports the shaft. Figure-2.5.1 (b) explains the essentials of the bearing model as presented by [28]. The two degree-of-freedom REB model captures the load-deflection relationships, while ignoring the effect of mass and the inertia of the rolling elements. The two degrees of freedom (x_s, y_s) are related to the inner race (shaft). Contact forces are summed over each of the rolling elements to give the overall forces on the shaft.

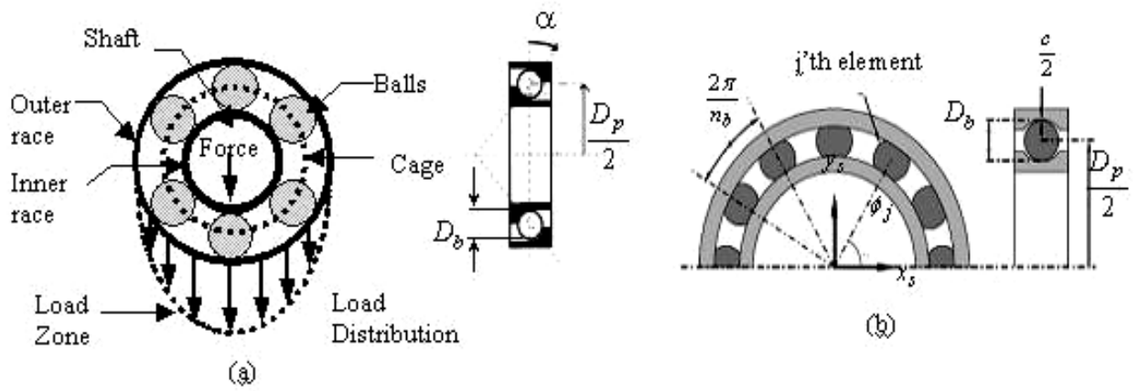

Fig. 2.5.1. (a) Rolling element bearing components and load distribution; (b) Two degree of freedom model. [28]

The overall contact deformation (under compression) for the j'th -rolling element δ_j is a function of the inner race displacement relative to the outer race in the x and y directions ($(x_s - x_p), (y_s - y_p)$), the element position ϕ_j (time varying) and the clearance (c). This is given by:

$$\delta_j = (x_s - x_p)\cos\phi_j + (y_s - y_p)\sin\phi_j - c - \beta_j C_d \quad (j = 1,2..) \tag{2.5.1}$$

Accounting for the fact that compression occurs only for positive values of δ_j, γ_j (contact state of δ_j the rolling elements) is introduced as:

$$\gamma_j = \begin{cases} 1, & if\ \delta_j > 0 \\ 0, & otherwise \end{cases} \tag{2.5.2}$$

The angular positions of the rolling elements ϕ_j are functions of time increment dt, the previous cage position ϕ_o and the cage speed ω_c (can be calculated from the REB geometry and the shaft speed ω_s assuming no slippage) are given as:

$$\phi_j = \frac{2\pi(j-1)}{n_b} + \omega_c dt + \phi_o \quad \text{with} \quad \omega_c = (1 - \frac{D_b}{D_p})\frac{\omega_s}{2} \tag{2.5.3}$$

The ball raceway contact force f is calculated by using traditional Hertzian theory (non-linear stiffness) from:

$$f = k_b \delta^n \tag{2.5.4}$$

The load deflection factor k_b depends on the geometry of contacting bodies, the elasticity of the material, and exponent n. The value of n=1.5 for ball bearings and n=1.1 for roller bearings. Using Equation-2.5.4 and summing the contact forces in the x and y directions for a ball bearing with n_b balls, the total force exerted by the bearings to the supporting structure can be calculated as follows:

$$f_x = k_b \sum_{j=1}^{n_b} \gamma_j \delta_j^{1.5} \cos\phi_j \quad \text{and} \quad f_y = k_b \sum_{i=1}^{n_b} \gamma_i \delta_j^{1.5} \sin\phi_j \tag{2.5.5}$$

The stiffness of the given REB model is non-linear, and is time varying as it depends on the positions of the rolling elements that determine the contact condition. The effect of slippage was introduced to the model by adding random jitters of 0.01-0.02 radians to the nominal position of the cage at each step.

2.5.2 Gearbox casing model – Component mode synthesis method

Lumped parameter modelling (LPM) is an efficient means to express the internal dynamics of transmission systems; masses and inertias of key components such as gears, shafts and bearings can be lumped at appropriate locations to construct a model. The advantage of the LPM is that it provides a method to construct an effective dynamic model with relatively small number of degrees-of-freedoms (DOF), which facilitates computationally economical method to study the behaviour of gears and bearings in the presence of nonlinearities and geometrical faults [32, 33, 34, 35].

One of the limitations of the LPM method is that it does not account for the interaction between the shaft and the supporting structure; i.e. casing flexibility, which can be an important consideration in light weight gearboxes, that are common aircraft applications. Not having to include the appropriate effect of transmission path also results in poor comparison between the simulated and measured vibration signals.

Finite Element Analysis (FEA) is an efficient and well accepted technique to characterize a dynamic response of a structure such as gearbox casings. However, the use of FEA results in a large number of DOF, which could cause some challenges when attempt to solve a vibro-dynamic model of a combined casing and the LMP of gearbox internal components. Solving a large number of DOFs is time consuming even with the powerful computers available today and it could cause a number of computational problems, especially when attempting to simulate a dynamic response of gear and bearing faults which involves nonlinearities.

To overcome this shortcoming, a number of reduction techniques [36, 37] have been proposed to reduce the size of mass and stiffness matrix of FEA models. The simplified gearbox casing model derived from the reduction technique is used to capture the key characteristics of dynamic response of the casing structure and can be combined with the LPM models of gears and REBs.

The Craig-Bampton method [37] is a dynamic reduction method for reducing the size of the finite element models. In this method, the motion of the whole structure is represented as a combination of boundary points (so called master degree of freedom) and the modes of the structure, assuming the master degrees of freedom are held fixed. Unlike the Guyan reduction [38], which only deals with the reduction of stiffness matrix, the Craig-Bumpton

method accounts for both the mass and the stiffness. Furthermore, it enables defining the frequency range of interest by identifying the modes of interest and including these as a part of the transformation matrix. The decomposition of the model into both physical DOFs (master DOFs) and modal coordinates allows the flexibility of connecting the finite elements to other substructures, while achieving a reasonably good result within a required frequency range. The Craig-Bumpton method is a very convenient method for modelling a geared transmission system as the input (excitation) to the system is not defined as forces, but as geometric mismatches at the connection points (i.e. gear transmission error and bearing geometric error). The following summary of the Craig-Bampton method is given based on the references [39-41].

In the Craig-Bampton reduction method, the equation of motion (dynamic equilibrium) of each superelement (substructure), without considering the effect of damping, can be expressed as in Equation-2.5.6:

$$[M]\{\ddot{u}\}+[k]\{u\}=\{F\} \tag{2.5.6}$$

Where $[M]$ is the mass matrix, $[k]$ is the stiffness matrix, $\{F\}$ is the nodal forces, $\{u\}$ and $\{\ddot{u}\}$ are the nodal displacements and accelerations respectively. The key to reducing the substructure is to split the degrees of freedom into masters $\{u_m\}$ (at the connecting nodes) and slaves $\{u_s\}$ (at the internal nodes). The mass, the stiffness and the force matrices are re-arranged accordingly as follows:

$$\overbrace{\begin{bmatrix} M_{mm} & M_{ms} \\ M_{sm} & M_{ss} \end{bmatrix}}^{M}\begin{Bmatrix} \ddot{u}_m \\ \ddot{u}_s \end{Bmatrix}+\overbrace{\begin{bmatrix} k_{mm} & k_{ms} \\ k_{sm} & k_{ss} \end{bmatrix}}^{k}\begin{Bmatrix} u_m \\ u_s \end{Bmatrix}=\begin{Bmatrix} F_m \\ 0 \end{Bmatrix} \tag{2.5.7}$$

The subscript m denotes master, s denotes slave. Furthermore, the slave degrees of freedom (internals) can be written by using generalized coordinates (modal coordinates by (q) using the fixed interface method, i.e. using the mode shapes of the superelement by fixing the master degrees of freedom nodes (connecting/ boundary nodes). The transformation matrix (T) is the one that achieves the following:

$$\begin{Bmatrix} u_m \\ u_s \end{Bmatrix}=T\begin{Bmatrix} u_m \\ q \end{Bmatrix} \tag{2.5.8}$$

For the fixed interface method, the transformation matrix (T) can be expressed as shown in Equation-2.5.9:

$$T=\begin{bmatrix} I & 0 \\ G_{sm} & \phi_s \end{bmatrix} \tag{2.5.9}$$

where,

$$G_{sm}=-k_{ss}^{-1}k_{sm} \tag{2.5.10}$$

and ϕ_s is the modal matrix of the internal DOF with the interfaces fixed.

By applying this transformation, the number of DOFs of the component will be reduced. The new reduced mass and stiffness matrices can be extracted using Equations 2.5.11 & 2.5.12 respectively:

$$M_{reduced} = T^t M T \tag{2.5.11}$$

and

$$k_{reduced} = T^t k T \tag{2.5.12}$$

Thus Equation-2.5.7 can be re-written in the new reduced form using the reduced mass and stiffness matrices as well as the modal coordinates as follows:

$$\overbrace{\begin{bmatrix} M_{bb} & M_{bq} \\ M_{qb} & M_{qq} \end{bmatrix}}^{M_{reduced}} \begin{Bmatrix} \ddot{u}_m \\ \ddot{q} \end{Bmatrix} + \overbrace{\begin{bmatrix} k_{bb} & 0 \\ 0 & k_{qq} \end{bmatrix}}^{k_{reduced}} \begin{Bmatrix} u_m \\ q \end{Bmatrix} = \overbrace{\begin{Bmatrix} F_m \\ 0 \end{Bmatrix}}^{F_{reduced}} \tag{2.5.13}$$

Where M_{bb} is the boundary mass matrix i.e. total mass properties translated to the boundary points. k_{bb} is the interface stiffness matrix, i.e. stiffness associated with displacing one boundary DOF while the others are held fixed. The M_{bq} is the component matrix (M_{qb} is the transpose of M_{bq}).

If the mode shapes have been mass normalized (typically they are) then:

$$k_{qq} = \begin{bmatrix} \backslash & & 0 \\ & \lambda_i & \\ 0 & & \backslash \end{bmatrix} \tag{2.5.14}$$

where λ_i is the eigenvalues; $\lambda_i = k_i / m_i = \omega^2{}_i$, and,

$$M_{qq} = \begin{bmatrix} \backslash & & 0 \\ & I & \\ 0 & & \backslash \end{bmatrix} \tag{2.5.15}$$

Finally the dynamic equation of motion (including damping) using the Craig-Bampton transform can be written as:

$$\begin{bmatrix} M_{bb} & M_{bq} \\ M_{qb} & I \end{bmatrix} \begin{Bmatrix} \ddot{u}_m \\ \ddot{q} \end{Bmatrix} + \begin{bmatrix} 0 & 0 \\ 0 & 2\zeta\omega \end{bmatrix} \begin{Bmatrix} \dot{u}_m \\ \dot{q} \end{Bmatrix} + \begin{bmatrix} k_{bb} & 0 \\ 0 & \omega^2 \end{bmatrix} \begin{Bmatrix} u_m \\ q \end{Bmatrix} = \begin{Bmatrix} F_m \\ 0 \end{Bmatrix} \tag{2.5.16}$$

where $2\zeta\omega$ = modal damping (ζ = fraction of critical damping)

For more detailed explanation of the techniques related to the modelling of rolling element bearings and the application of component mode synthesis (CMS) techniques, refer to the works by Sawalhi, Deshpande and Randall [41].

2.6 Solving the gear dynamic simulation models

A block diagram summarizing the time integral solution of a typical dynamic model with some time varying parameters is shown in Figure-2.6.1. There are a range of numerical algorithms available today to give solution of the dynamic models: direct time integration, harmonic balancing and shooting techniques, to name some commonly recognized methods.

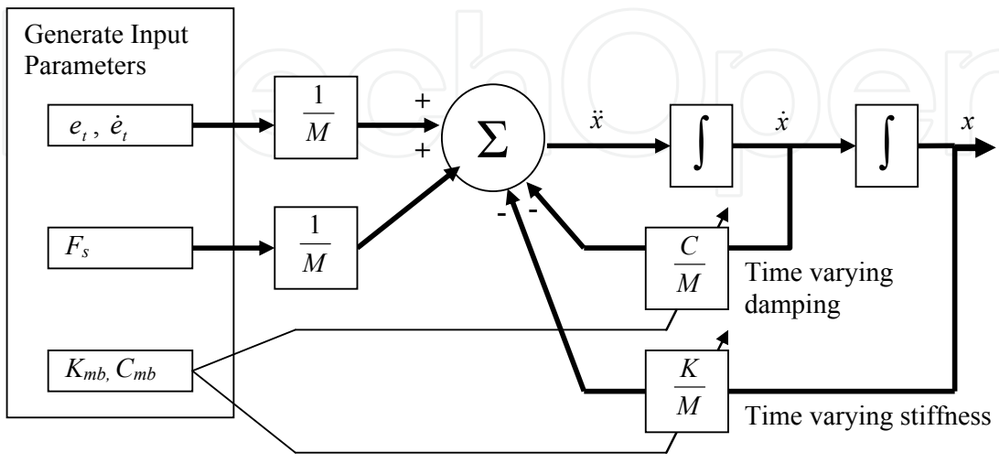

(NOTE: '∫' stands for integration over a single step of incremented time)

Fig. 2.6.1. Dynamic Simulation Process

Sometimes the solution for gears requires simulation of highly non-linear events, for example, rattling and knocking in gears, which involve modelling of the contact loss. The works presented by R. Singh [42], Kahraman & Singh [43], Kahraman & Blankenship [18] and Parker & Lin [9, 10] show some examples of the "stiff" problems involving non-linearity due to contact loss and clearances.

The solution for these Vibro-Impact problems presents difficulties involving ill-conditioning and numerical "stiffness". In [42] Singh explains that ill-conditioning of a numerical solution occurs when there is a component with a large frequency ratio: ratio of gear mesh frequency to the natural frequency of the component.

The numerical stiffness in the gear dynamic simulation becomes a problem when gears lose contact. The relationship between the elastic force, relative deflection and gear mesh stiffness is illustrated in Figure-2.6.2. The gradient of the curve represent the gear mesh stiffness.

Contact loss between the gears occurs when the force between the gears becomes zero. The gears are then unconstrained and free to move within the backlash tolerance. The presence of a discontinuity becomes obvious when the derivative of the curve in Figure-2.6.2 (i.e. mesh stiffness) is plotted against the relative deflection. The discontinuity in the stiffness introduces instability in the numerical prediction.

In more formalized terms the "stiffness" of a problem is defined by local Eigen-values of the Jacobian matrix. Consider an equation of motion expressed in simple first order vector form '$f(x, t)$', (Equation-2.6.1). Typically, the solution of an equation of motion is obtained by linearizing it about an operating point, say 'x_0', (Equation-2.6.2). Usually, most of the higher

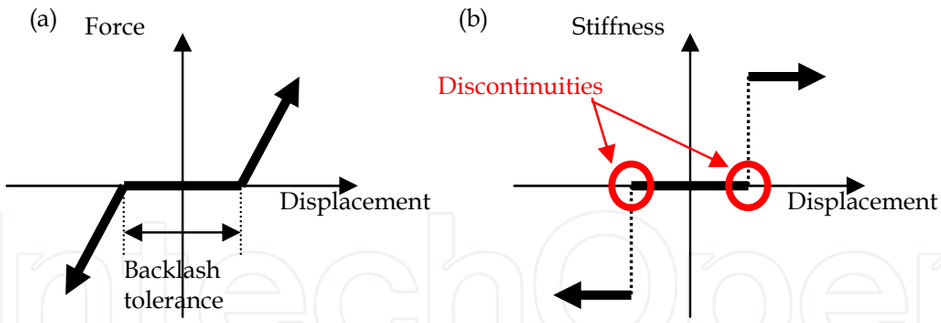

Fig. 2.6.2. Non-linearity due to contact loss in meshing gears; a) Force vs. Displacement, b) derivative of former, i.e. Stiffness vs. Displacement

order terms above the 1st derivative are ignored for linearization, which leaves the following expression (Equation-2.6.3). The differential term '***J***' is called the Jacobian matrix (or Jacobian in short). The problems involving gear contact losses are "Stiff" problems because of the discontinuity in system derivatives (Jacobians). For a more detailed discussion on this topic refer to the work presented by Singh [42].

$$\underline{f}(x,t) = {}^{dx}\!/_{dt} \tag{2.6.1}$$

$$\underline{f}(x,t) \cong \underline{f}(x_0,t) + \left({}^{df}\!/_{dx}\right)_{x_0} (x - x_0) \tag{2.6.2}$$

$$\underline{f}(x,t) \cong \underline{f}(x_0,t) + \underline{J}(x - x_0) \tag{2.6.3}$$

3. Modelling gearbox faults

The study of gear faults has long been an important topic of research for the development of gear diagnostic techniques based on vibration signal analysis. Understanding how different types of gear tooth faults affect the dynamics of gears is useful to characterise and predict the symptoms of the damage appearing in vibration signals [44, 45]. The strong link between the TE and the vibration of the gears was explained earlier. The effect of different types of gear tooth faults on TE can be studied by using the static simulation models. The result of static simulation can be then used to determine how different types of gear faults can be modelled into the dynamic simulation.

Gears can fail for a broad range of reasons. Finding a root cause of damage is an important part of developing a preventative measure to stop the fault from recurring. Analysis of gear failure involves a lot of detective works to link the failed gear and the cause of the damage. Comprehensive guidelines for gear failure analysis can be found in Alban [46], DeLange [47] and DANA [48]. AGMA (American Gear Manufacturers Association) recognizes four types of gear failure mode and a fifth category which includes everything else: Wear, Surface Fatigue, Plastic Flow, Breakage and associated gear failures [49].

The effect of gear tooth fillet cracks (TFC) and spalls on gear transmission error was studied in detail by using a static simulation models (FEA and LTCA (HyGears [50])). A pair of meshing gears were modelled and analysed in step incremented non-linear static environment. Note: the transmission error obtained from the static simulation models are referred to as Motion Errors (ME) here forth by following the HyGears convention.

It was explained earlier that the interaction between two meshing gears can be expressed in the dynamic model as time-varying stiffness, damping and gear tooth topological error elements linking the two lumped mass moments of inertia. The effect of gear tooth faults can be implemented into the dynamic simulation model as changes to these parameters. The understanding gained from the detailed simulation model studies of TFCs and spalls on gear motion has lead to the method of modelling the effect of the faults in dynamic model. The relevance between the types of gear faults to the selected parameters will be explained through subsequent sections.

Further to the simulation of gear tooth faults, this chapter also briefly touches on the modelling of spalls in rolling element bearings (REB), which is also a common type of faults in geared transmission systems.

3.1 Modelling the effect of a fatigue crack in tooth fillet area of a gear

Classical tooth root fillet fatigue fracture is the most common cause of gear tooth breakages (Figure-3.1.1). Stress raisers, such as micro cracks from the heat treatment, hob tears, inclusions and grinding burns are common causes that initiate the cracks. The cracks occurring in the gear tooth fillet region progressively grow until the whole tooth or part of it breaks away. The breakage of a tooth is a serious failure. Not only the broken part fails, but serious damage may occur to the other gears as a result of a broken tooth passing though the transmission [48].

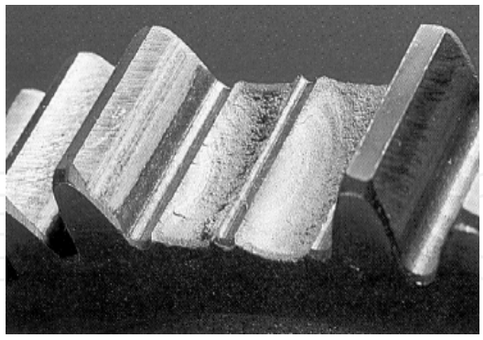

Fig. 3.1.1. A spur gear missing two teeth. They broke away due to the propagation of fatigue cracks. (Courtesy of DANA [48])

The research conducted for NASA by Lewicki [51] sets a clear guideline for predicting the trajectory of cracks occurring at the gear tooth fillet. Lewicki predicted crack propagation paths of spur gears with a variety of gear tooth and rim configurations, including the effect of: rim and web thickness, initial crack locations and gear tooth geometry factors (Diametral pitch, number of teeth, pitch radius and tooth pressure angle). A summary of the results is presented in Figure-3.1.2.

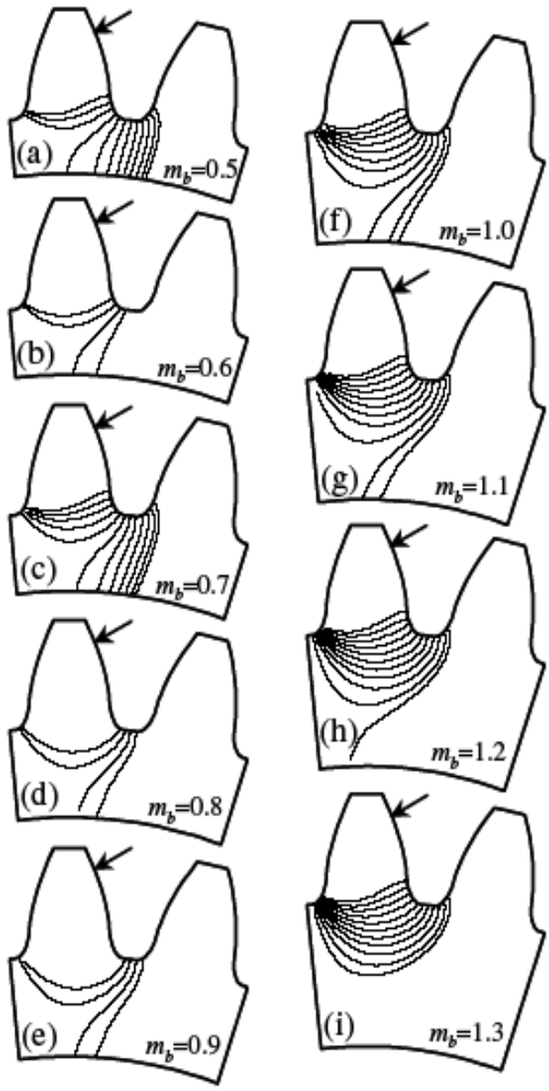

Fig. 3.1.2. Effect of backup ratio (m_b) and initial crack location on propagation path. (Lewicki [51])

A set of spur gears later used in the validation of the simulation result have a "backup ratio" (rim thickness divided by tooth height) greater than m_b=1.3. Therefore based on the Lewicki's prediction the cracks occurring in the tooth fillet region are most likely to propagate in the trajectory shown in Pattern Figure-3.1.2 (i); roughly 30~45° in to the tooth relative to the radial line path through the symmetric axis of the spur gear tooth profile.

Full 3D modelling of a propagating gear tooth crack is one of the actively researched areas. Some examples of simulation studies using the Boundary Element Method (BEM) are given in [52, 53, 54, 55]. The simulation studies using 3D models show complex behaviour crack growth from the small crack seeded at the middle of the gear tooth fillet. An example is shown in Figure-3.1.3 from "Modelling of 3D cracks in split spur gear", by Lewicki [52]. The crack front expands rapidly across the width of the gear tooth as it progresses into the thickness of the tooth. The tooth fillet crack (TFC) model used in this work assumes 2D

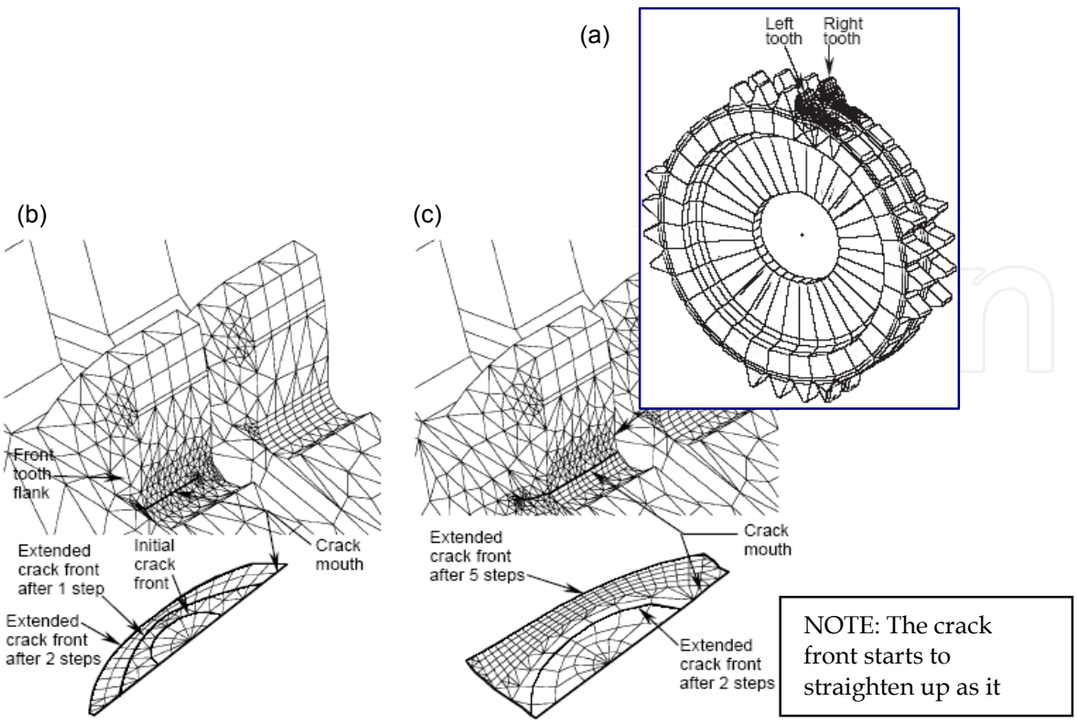

Fig. 3.1.3. 3D Crack propagation model. a) Boundary Element Model of Split Spur Gear, b) Close up of view of the gear teeth and crack section at earlier stage of development and c) more progressed crack. (Lewicki [53])

conditions which approximates the weakening of the cracked gear tooth when the crack is extended across the whole width of the tooth face.

The motion error $(ME)_t$ as obtained from the finite element (FE) model of a gear pair (32x32 teeth) presented in Figure-3.1.4, is shown in Figure-3.1.5. The MEs of the gears at different

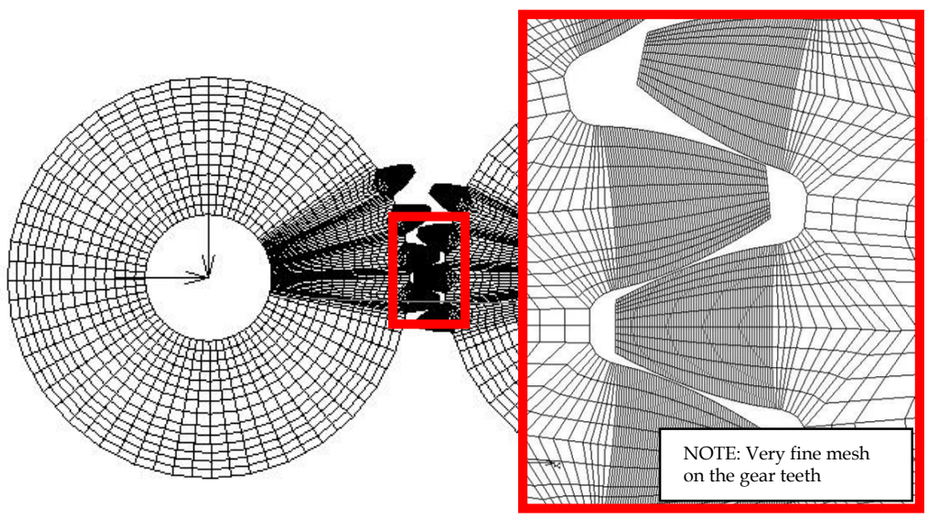

Fig. 3.1.4. Spur Gears (32x32) and its FE mesh (L), detailed view of the mesh around the gear teeth (R). [56]

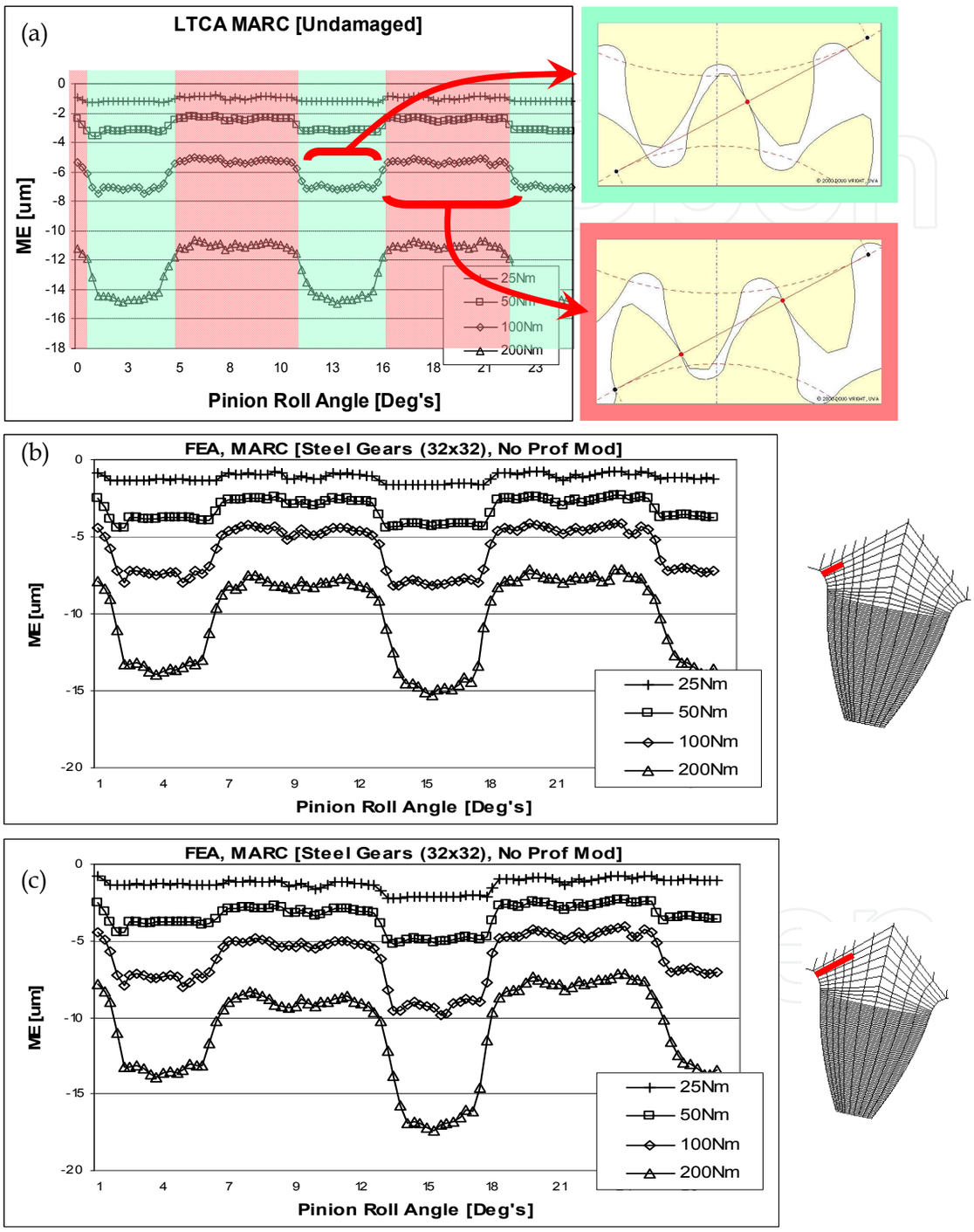

Fig. 3.1.5. Motion Errors of (32x32) teeth gear pairs; (a) Undamaged gear set; (b) TFC (L=1.18mm); (c) TFC (L=2.36mm)

amount of loadings (25, 50, 100 & 200Nm) are compared in the same plot. The magnitude of MEs increases with the larger loads as the deflection of the meshing teeth become greater with the larger loads. The change in the amount of ME is roughly in linear relationship with the load, which reflects the linear elastic behaviour of the gear tooth deflection. Note the square pattern of the ME, which resulted from the time (or angular position) dependent variation of gear mesh stiffness, due to the alternating single and double tooth engagement.

The plots presented in Figures 3.1.5 (b) & (c) show the MEs of the gears with tooth fillet cracks of three different sizes. The localized increase in the amount of ME over a period of ME pattern is a direct consequence of the reduced gear tooth stiffness caused by the TFC.

The plots shown in Figure-3.1.6 (a) ~ (c) are the residual ME (RME) obtained by taking the difference between the MEs of uncracked gears and the ones with TFCs. The RMEs show a "double stepped" pattern that reflects the tooth meshing pattern of the gears, where smaller step with less deflection occurs as the crack tooth enters the mesh and share the load with the adjacent tooth; the larger second step follows when the cracked tooth alone carries the load.

The RMEs of the TFCs show linearly proportional relationship between the amount of loading and the change in RME for a given crack size. The linear relationship between the loading and the amount of tooth deflection on a cracked gear tooth indicates that the effect of TFC can be modelled effectively as a localized change in the gear mesh stiffness.

The plots in Figure-3.1.7 show the transmission errors (TEs) measured from a pair of plastic gears with a root fillet cut (Figure-3.1.7 (a)), which the cut replicates a tooth fillet crack. The TEs of Figure 3.1.7 (c1-c3 and d1-d3) are compared to the simulated patterns of MEs (figure 3.1.7 (b)). Composite TEs (CTEs) and the zoomed view of the CTEs are shown in Figure-3.1.7 (c1 & d1) and (c2 & d2) respectively. The CTE combines the both long and short term components of the TE (LTC and STC) presented earlier in section 2.2 (figure 2.2.1). The resemblance between the simulated MEs and measured the TEs confirms the validity of the simulated effect of TFC. The STCs (c3 & d3) were obtained by high pass filtering the CTE. The pattern in the STCs shows clear resemblance to the simulated TFC effect (Figure3.1.7 (b)).

The simulation model used in this study does not consider the effect of plasticity. This assumption can be justified for a gear tooth with small cracks where localised effect of plasticity at the crack tip has small influence on the overall deflection of the gear tooth, which is most likely the case for the ideal fault detection scenario.

More recent work published by Mark [57, 60] explains that the plasticity can become a significant factor when work hardening effect can cause a permanent deformation of the cracked tooth. In this case, the meshing pattern of the gears changes more definitively by the geometrical error introduced in the gears by the bent tooth. In some cases the bent tooth result in rather complex meshing behaviour that involves tooth impacting. Further explanation on this topic is available from the works published by Mark [57, 60].

Within the limitation of the simulated TFC model discussed above, the approach to model the TFC as a localized variation in the gear mesh stiffness is acceptable for a small crack emerging in the gear tooth fillet area. For the purpose of developing a dynamic simulation model of a geared transmission system with an emerging TFC the model presented here offers a reasonable approach.

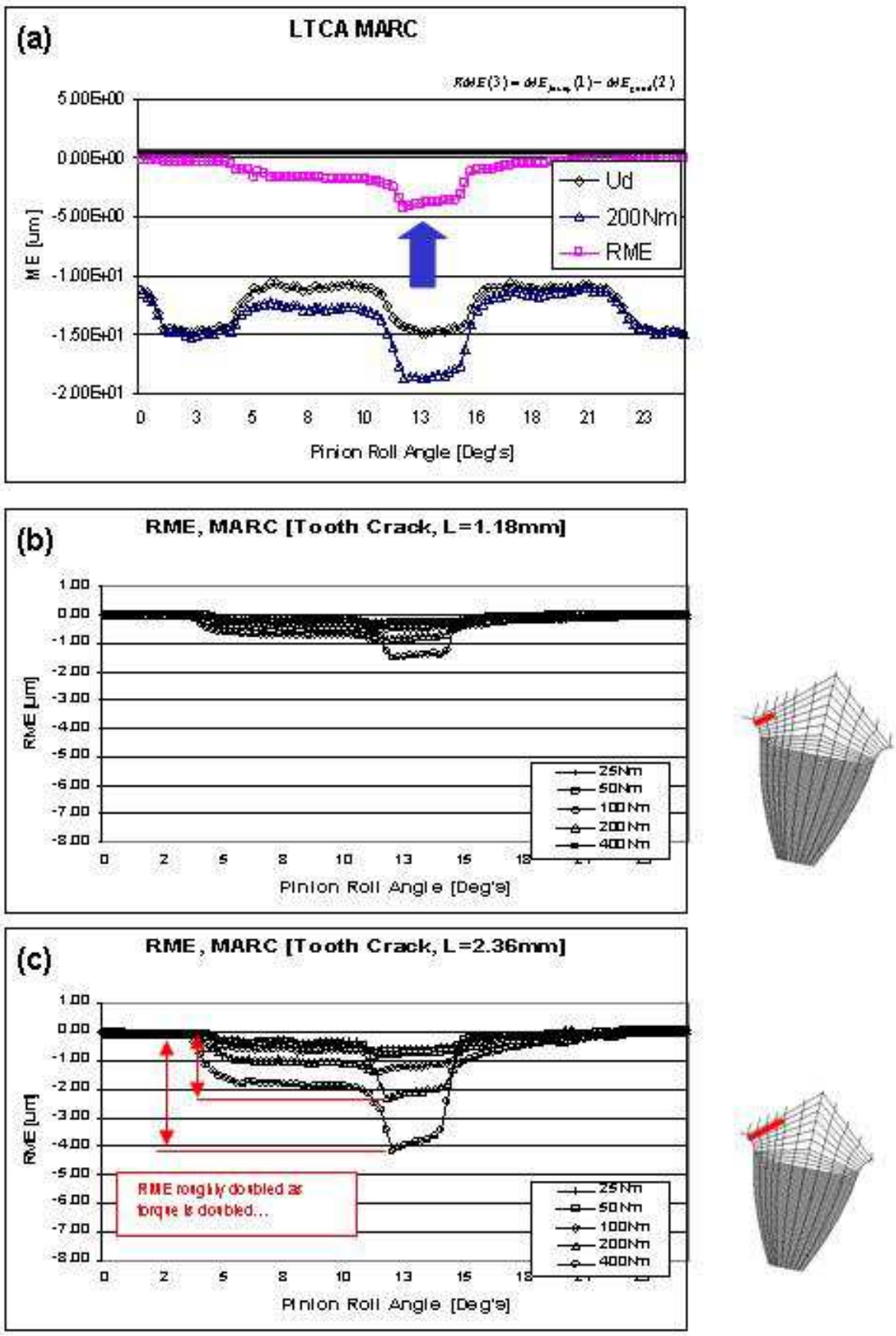

Fig. 3.1.6. Comparison of RMEs of gears with TFCs; (a) Illustrated definition of RME; (b) RMEs of TFC sizes L=1.18mm; (c) RMEs of TFC sizes L=2.36mm.

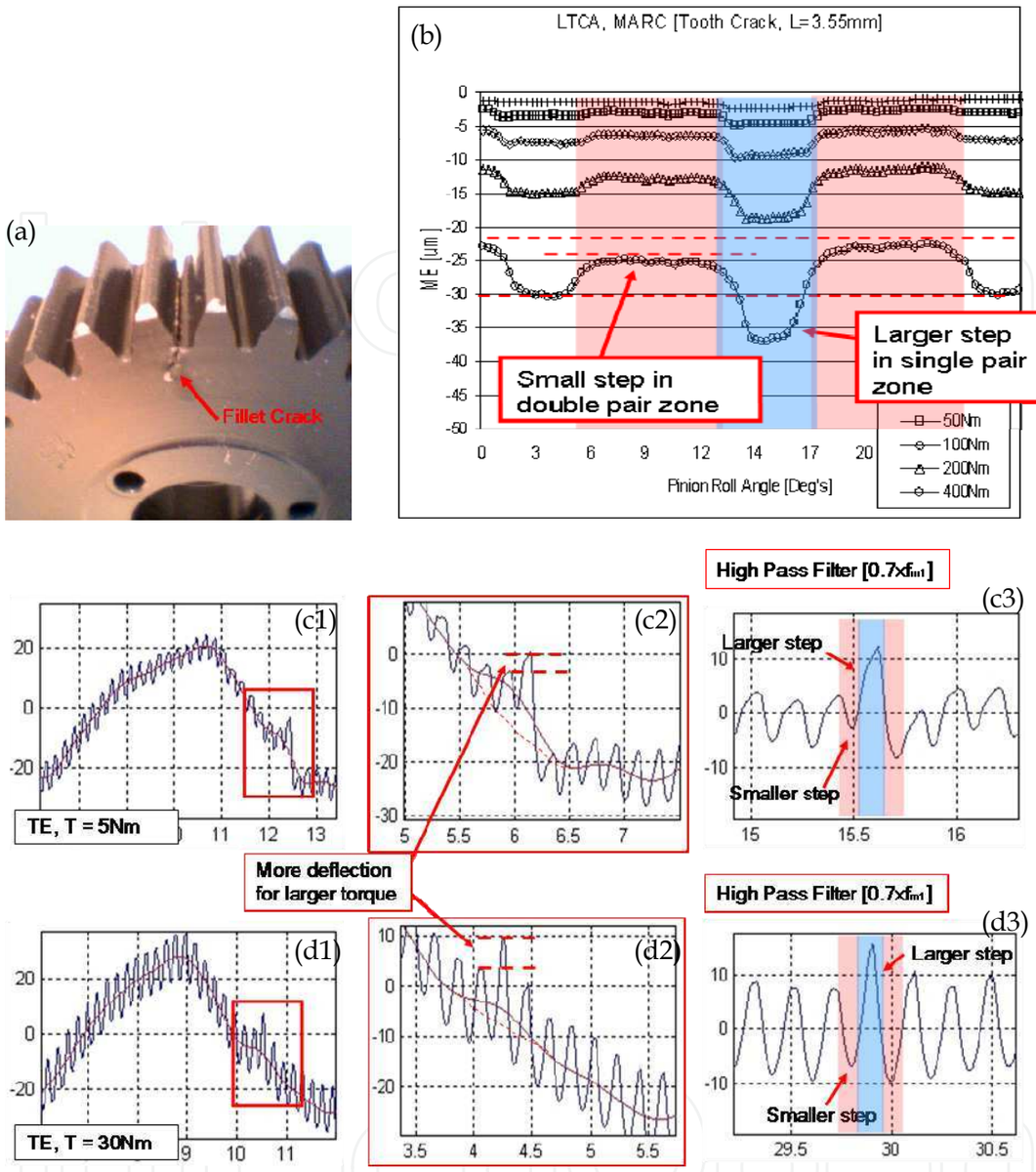

Fig. 3.1.7. Comparison of simulated vs. measured transmission errors; (a) Picture of a gear with a seeded TFC; (b) MEs from a FE model. (c1) ~ (c3) TEs of the gears with TFC loaded with 5Nm; (d1) ~ (d3) TEs of the gear with TFC loaded with 30Nm; CTE (c1, d1), Zoomed views (c2, d2) and STC (c3, d3).

3.2 Modelling the effect of a spall on a tooth face of a gear

Symptoms of surface fatigue vary, but they can generally be noticed by the appearance of cavities and craters formed by removal of surface material. The damage may start small or large and may grow or remain small. In some cases gears cure themselves as they wear off the damage: Initial pitting [47]. The terms "Spalling" and "Pitting" are often used indiscriminately to describe contact fatigue damages. Figure-3.2.1 shows some examples of

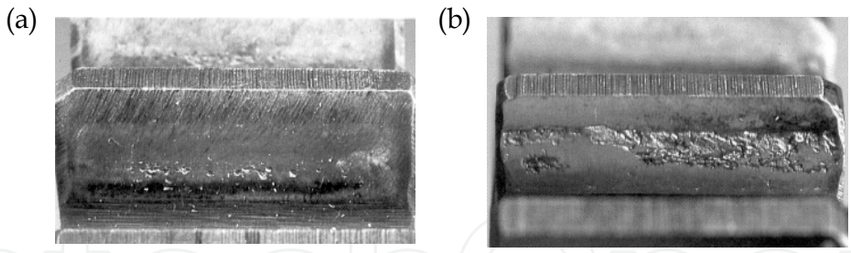

Fig. 3.2.1. Examples of (a) progressive pitting and (b) severe spalling damages on gear teeth. (DANA [48])

spalls and pitting occurring on a gear tooth. This work follows the definition of contact surface damage given by Tallian [58]: Spalling designated only as macro-scale contact fatigue, reserving the term pitting for the formation of pores and craters by processes other than fatigue cracking.

There are three distinctive phases in the development of surface fatigue damage:

1. Initial Phase: Bulk changes in the material structure take place around the highly stressed area under the contact path. Change in hardness, residual stress and some microscopic changes in the grain structure of the metal.
2. A Long Stable Phase: Microscopic flow occurs in the highly stressed area changing the material structure and residual stress conditions at the microscopic level. The change in the structure brought out by the microscopic flow can be observed by eyes in the illuminated etched areas.
3. Macroscopic Cracking: This is the last failure phase instituting the crack growth.

Spalls have a distinctive appearance that is characterised by how they were formed. A fully developed spall typically has its diameter much larger than its depth. The bottom of the spall has a series of serrations caused by propagating fatigue cracks running transverse to the direction of rolling contact. The bottom of the spall parallels the contact surface roughly at the depth of maximum unidirectional shear stress in Hertzian contact.

The sidewalls and the wall at the exiting side of the spall (as in the exiting of rolling contact) are often radially curved as they are formed by material breaking away from the fatigued area. The entrance wall of the spall is characterised by how it was initiated. Tallian [58] explains that shallow angled entry (less than 30˚ inclination to the contact surface) occurs when the spall is initiated by cracks on the surface. Spalls with steep entry (more than 45˚) occur when the spall is initiated by subsurface cracks.

Surface originated spalls are caused by pre-existing surface damage (nicks and scratches). It is also known that lubrication fluid could accelerate the crack propagation when contact occurs in such a way that fluid is trapped in the cracks and squeezed at extremely high pressure as the contacting gear teeth rolls over it.

The subsurface originated spalls are caused by presence of inclusions (hard particles and impurities in the metal) and shearing occurs between the hard and the soft metal layers formed by case hardening. A spall caused by the initial breakage of the gear tooth surface continues to expand by forming subsequent cracks further down the rolling direction. Figure-3.2.2 illustrates the formation and expansion of spall damage by Ding & Rieger [59].

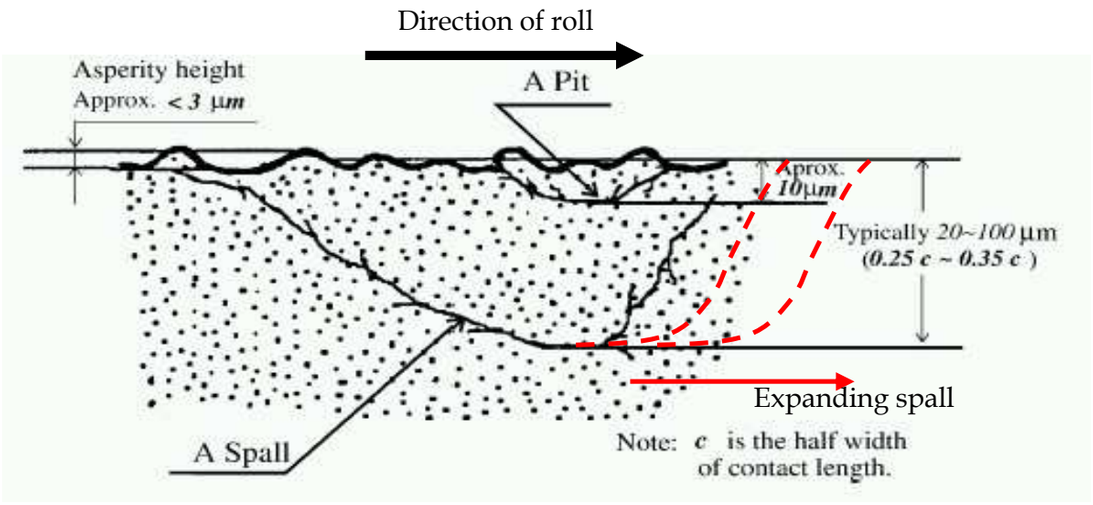

Fig. 3.2.2. Formation and expansion of spalls. (Ding & Rieger [59])

The result of contact stress analysis from HyGears [50] shows the occurrence of high stress concentration at the entrance and exit walls of the spall (Figure-3.2.3). The high stress concentration at these edges implies the likelihood of damage propagation in that direction. The result of the simulation corresponds to Tallian's [58] observation that spalls tend to expand in the direction of rolling contact. In the HyGears simulation the spall was modelled as a rectangular shaped recess on the tooth surface in the middle of the pitch line.

Typical spur gear tooth surfaces are formed by two curvatures: profile and lead curvatures. The 2D models are limited to simulating the effect of the spall crater on the gear tooth profile only. 3D simulation is required to comprehend the complete effect of spalls on the

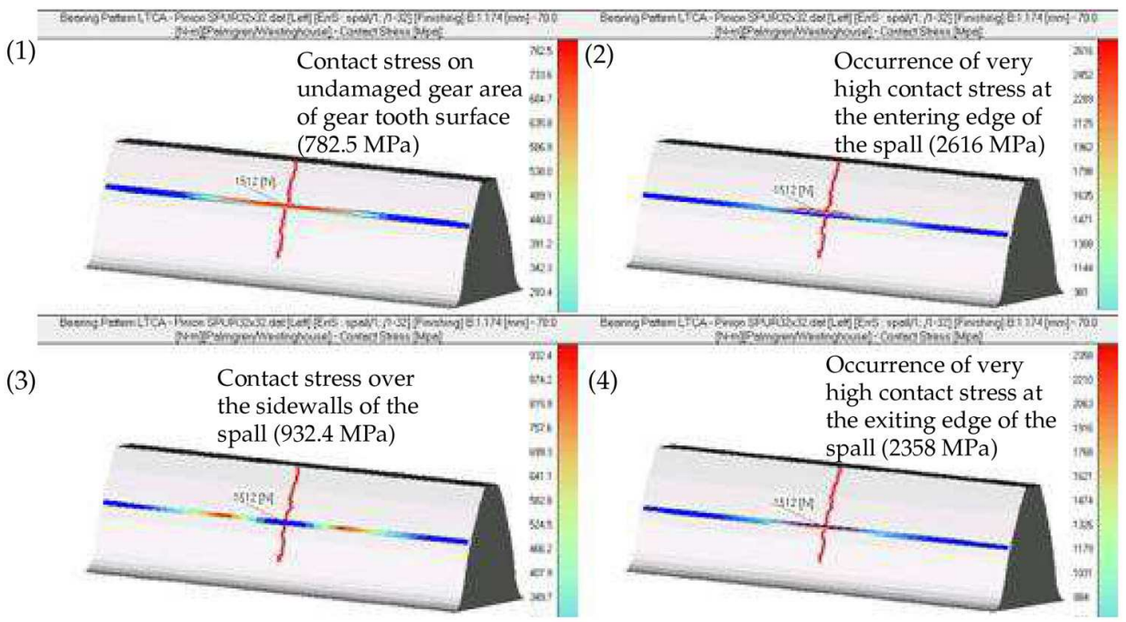

Fig. 3.2.3. HyGears analysis of contact stresses around the spall. [62]

contact surface of the gears. A study was carried out to investigate the effect of spalls on the ME using a 3D gear tooth model [62]. The result of the study showed that the effect of the spalls on the ME is completely dominated by the displacement caused by the topological error of the gear tooth surface caused by the fault.

Formation of spalls is a complicated process and it is one of the active research topics which have been studied for some time. Although there are several items in the literature that describe the properties and process of formation of spalls, no literature was sighted which defines the specific definition of shapes and sizes of spalls occurring on spur gear teeth.

Papers presented by Badaoui et al. [63, 64] and Mahfoudh et al. [65] show a successful example of simulating the effect of a spall on spur gear tooth by modelling the fault as prismatic slot cut into the gear tooth surface. Their results were validated by experiment. The model of the spall used in this work follows the same simplification of the general shape of the spalling fault. The simulation of the spall is bounded by these following assumptions:

1. A spall is most likely to initiate at the centre of the pitchline on a gear tooth where maximum contact stress is expected to occur in the meshing spur gear teeth as the gears carry the load by only one pair of teeth.
2. The spall expand in size in the direction of rolling contact until it reaches the end of the single tooth pair contact zone as shown in Figure-3.2.4.
3. When the spall reaches the end of the single tooth pair contact zone, the spall will then expand across the tooth face following the position of the high contact stresses. The contact stress patterns shown in Figure-3.2.3 strongly support this tendency of spall growth.

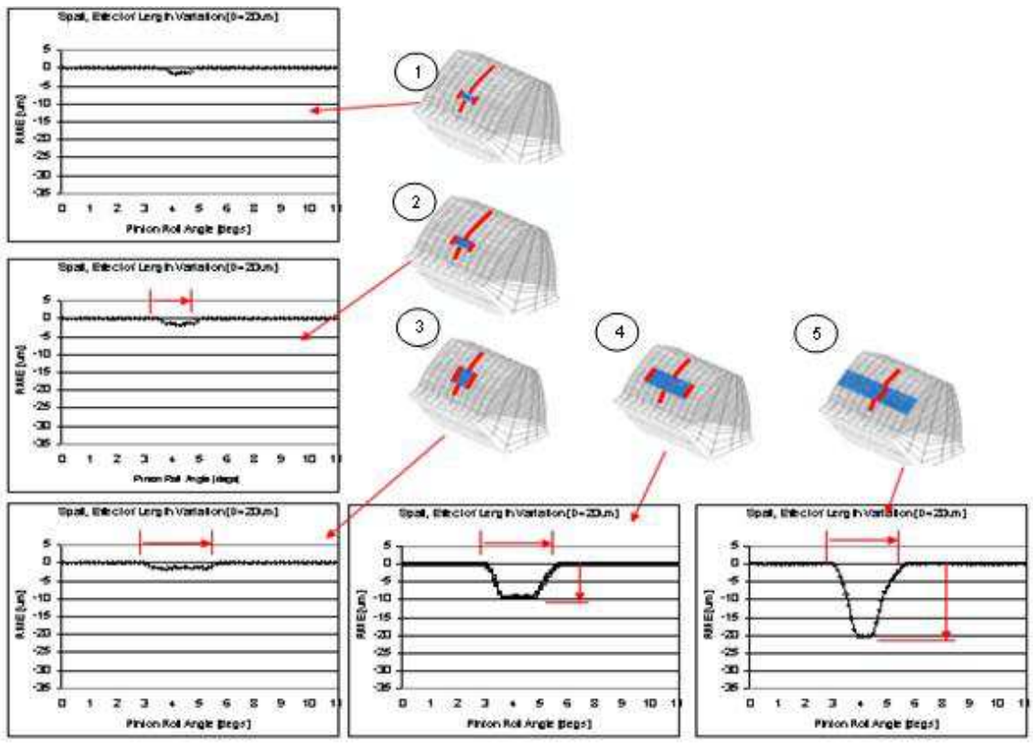

Fig. 3.2.4. A model of spall growth pattern and the resulting RME. [62]

The models of spalls were developed by following the set of assumptions described above. Resulting plots of the RMEs are presented in Figure-3.2.4 along with the shape illustration of spalls on a gear tooth. Note that the RMEs of the spalls form bucket shapes and their length and the depth are determined by the length and width of the spall; i.e. the shape of RME and the progression of the spall is directly related. This information can be used in diagnosis and prognosis of the fault.

The plots in Figure-3.2.5 show TEs measured from a pair of plastic gears with a spall (Figure-3.2.5 (a)). The change in the pattern of the TE due to the spall is comparable to the simulated pattern of the MEs (Figure-3.2.5 (b)). Composite TEs (CTEs) and the zoomed views of the CTEs are shown in Figure-3.2.5 (c1~c3). The resemblance between the simulated MEs and measured TEs confirms the validity of the simulated effect of TFC. The STCs (d1~d3) were obtained by high pass filtering the CTE. The pattern in the STCs shows clear correlation between the simulated and measured patterns of spall motion errors.

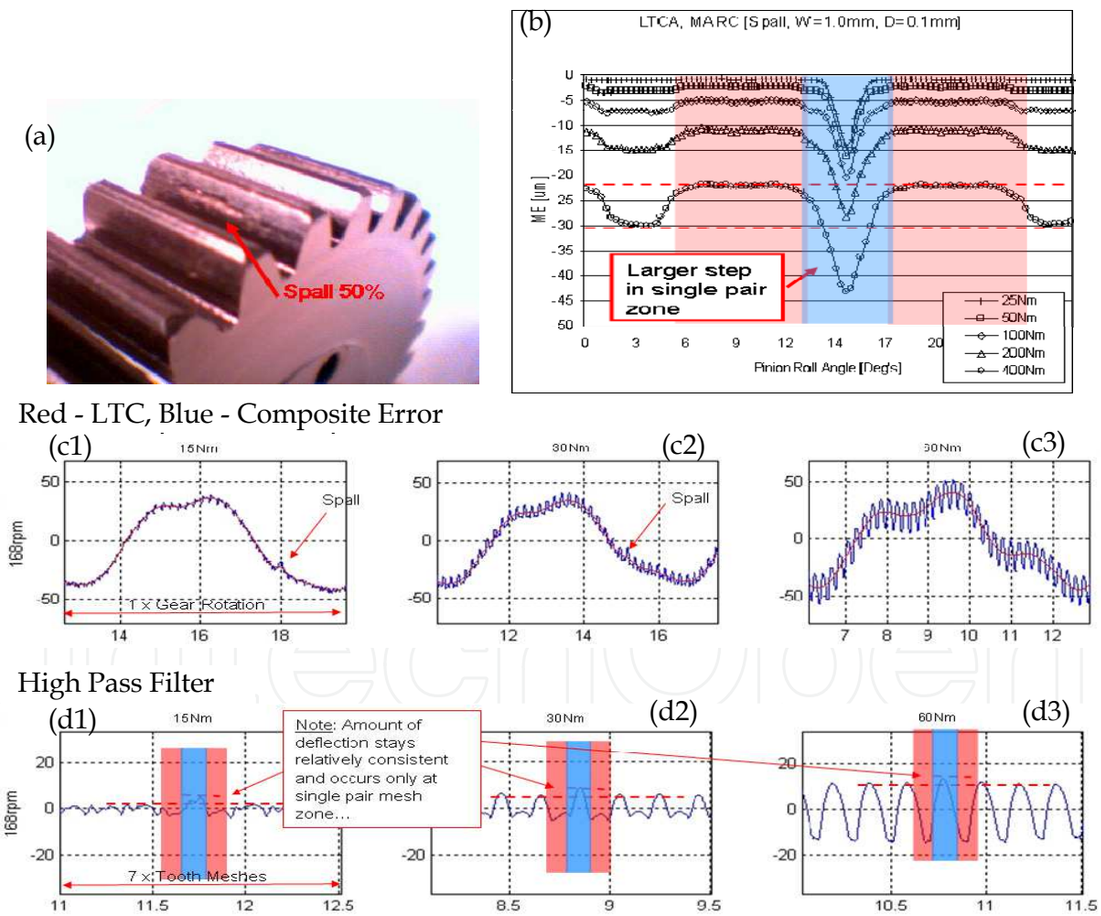

Fig. 3.2.5. Comparison of simulated vs. measured transmission errors; (a) Picture of a gear with a seeded Spall; (b) MEs from a FE model; (c1) ~ (c3) CTEs of the gear with the spall; (d1) ~ (d3) STCs of the gear with the spall; Applied torque: 15Nm (c1 & d1), 30Nm (c2, d2), 60Nm (c3, d3).

3.3 Simulating the effect of TFCs and spalls in a gear dynamics model

The FEA model based study of TFCs and spalls has lead to identifying some useful properties of the faults that can be used to model the effect of the faults in the lamped parameter type gear dynamics models.

The Residual Motion Errors (RME) of TFCs have shown double stepped patterns that were load dependent. The change in the amount of deflection in the gear mesh (i.e. ME) with a cracked tooth is influenced by the size of the crack and also by the amount of loading on the gears. The simulation result showed that the linearly proportional relationship between the torque applied to the gears and the resulting RME value. The bucket shaped RMEs of spalls were not affected by the loading condition but purely driven by the change in the contact path patterns of the meshing teeth, due to the geometrical deviation of the gear tooth surface caused by a spall. It was also understood from the simulation studies that the size and the shape of a spall affect the length and the depth of the bucket.

Based on the observation above, the effect of TFC was modelled as locally reduced tooth meshing stiffness and the spalls as direct displacement due to the topological alteration of the gear tooth surface. In the gear dynamic model is shown in Figure-3.3.1, the effect of a TFC was implemented as a reduction in stiffness "K_m" over one gear mesh cycle. The change in the value of K_m was calculated from the FEA model mapped into an angular position dependent function in the gear dynamic model. A spall was implemented as a localized displacement mapped on the "e_t". An illustration of a TFC and a spall models in a gear rotor dynamic model is shown in Figure-3.3.1 [61].

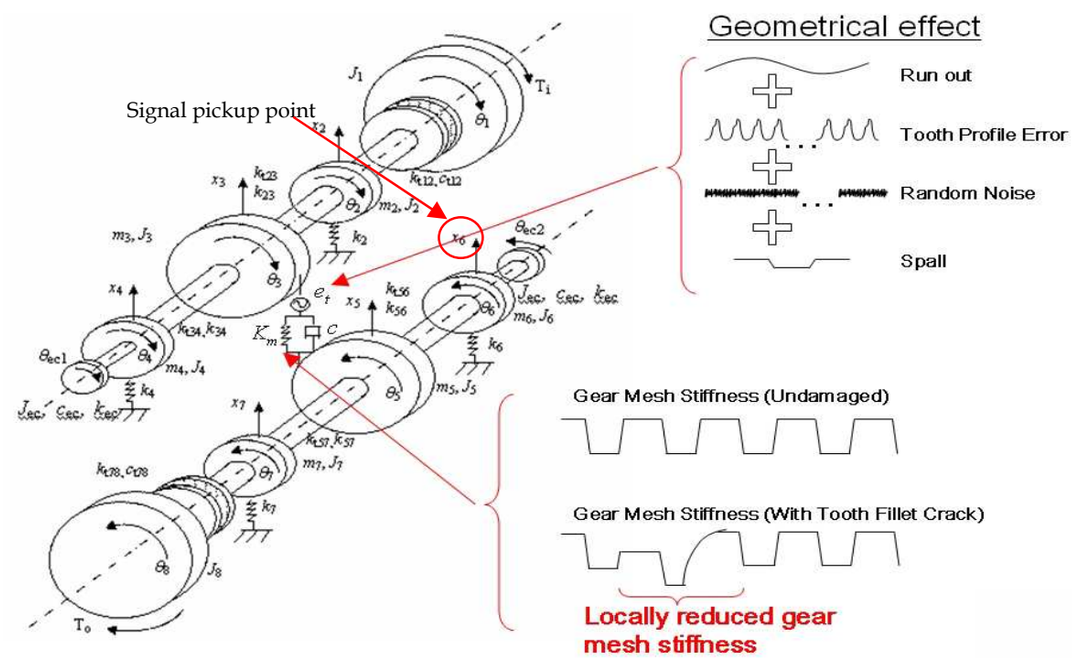

Fig. 3.3.1. Modelling of Gear Tooth Faults in Dynamic Model. [61]

Figures 3.3.2 (a1~a3) and 3.3.3 (a1~a3) show the simulated vibration signal (acceleration) from the LPM shown in the Figure-3.3.1. The signals were measured from the free end of the

driven shaft (see Figure-3.3.1). The residual signals shown in (b1~b3) of Figures 3.3.2 and 3.3.3 were obtained by subtracting the simulated vibration of undamaged gearbox from the damaged one. Two identical simulation models, one with a gear tooth fault (TFC or spall) and the other undamaged, were run in parallel and the difference between the two model out puts were taken to separate the effect of the gear faults. The impact like effect of the gear tooth faults is seen in both the gears with a TFC and a spall.

A comparison of the simulated signals shows that the magnitude of the TFC impulses is affected by the amount of torque applied to the gears, while the spall impulses are not. This response is consistent with the observation made in the static simulation of the gears in mesh.

Careful observation of the residual signal also reveals that the fault information is not only buried in the dominant effect of gearmesh, but also somewhat distorted by the effect of transmission path from the gearmesh to the point where the signal was measured. The effect of transmission path appears in the residual signal As the transient "tail" effect convolved over the impulse due to the gear fault (see Equation-3.3.1 and Figure-3.3.4 for illustration).

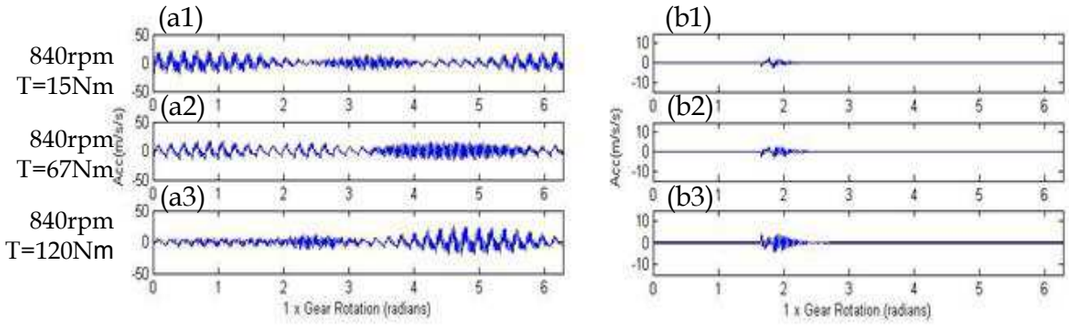

Fig. 3.3.2. Simulated gearbox vibration signal with the effect of a TFC.

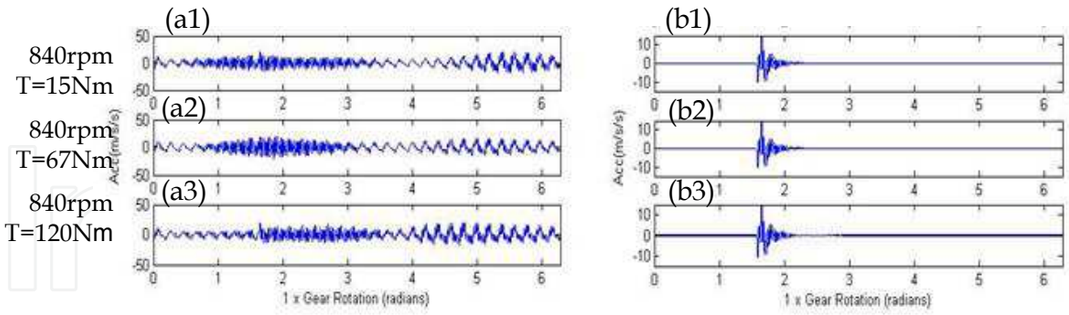

Fig. 3.3.3. Simulated gearbox vibration signal with the effect of a spall.

The residual signal of the TFC and the spall provide a useful means to understand the nature of diagnostic information of the faults. In machine condition monitoring signal processing techniques are often developed to detect and quantify the symptoms of a damage buried in a background noise. By being able to see the "clear" effect of a fault, the most effective signal processing technique can be applied to target and monitor the symptoms of the damage. The idea of using the simulated fault signals to design and improve the fault detection and machine condition monitoring techniques has been put to effective uses by Randall, Sawalhi and Endo [34, 35, 62, 66].

$$y = (e + w + n) * h \quad \text{(Note: * represents convolution)} \tag{3.3.1}$$

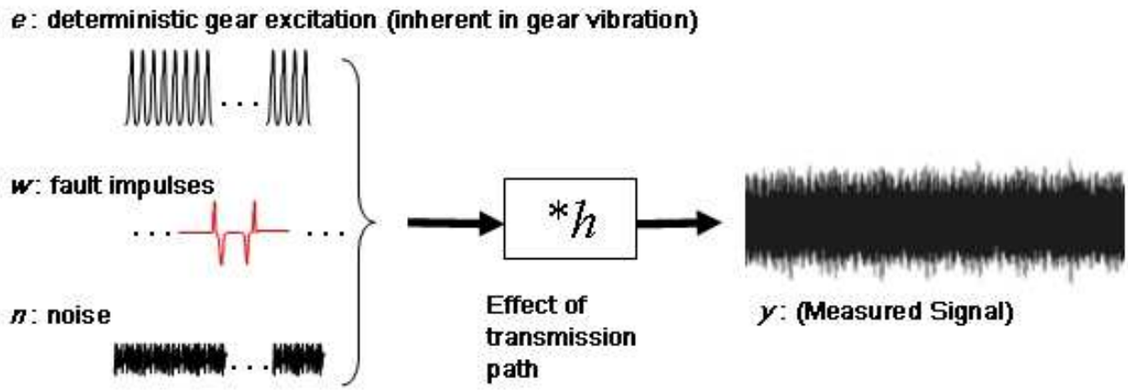

Fig. 3.3.4. Vibration of a Gearbox. [62]

3.4 Modelling a spall in a rolling element bearing

This section discusses a several simple but an effective methods of modelling a spall in the rolling element bearing model introduced previously in section 2.5.1. The ideas behind each modelling approach was discussed by using the example of modelling a spall in the outer race of a bearing. The same method can be easily expanded in to modelling an inner race spall and ball faults. More detailed explanation on this topic is available from the work published by Sawalhi and Randall [29, 30, 31, 34, 35, 66, 67].

The simplest form of a spall model can be implemented to the REB model by assuming instantaneous contact loss between the bearing races and rollig an element(s) as it pass over the spall. So, in reference to the rolling element model described above, the presence of a spall of a depth (C_d) over an angular distance of ($\Delta\phi_d$) can be modelled by using the fault switch β_j which defines the contact state of rolling elements over a defined angular position (ϕ_d). In effect, this mothod models the spall as a step function as shown in Figure-3.4.1 and further illustrated by Figure-3.4.2 (a), in which β_j is defined as follows:

$$\beta_j = \begin{cases} 1, & if\ \phi_d < \phi_j < \phi_d + \Delta\phi_d \\ 0, & otherwise \end{cases} \tag{3.4.1}$$

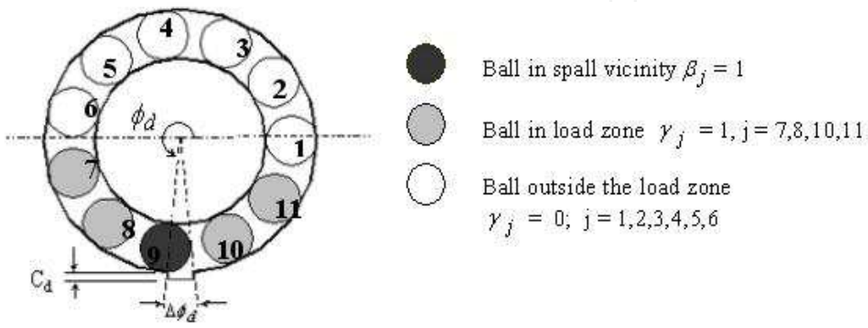

Fig. 3.4.1. Spall definition on the outer race [66]

Fig. 3.4.2. Modified model of a spall based on a more realistic ball trajectory. [66]

The outer race spall is fixed in location between ϕ_d and $\phi_d + \Delta\phi_d$. This normally occurs in the load zone. An inner race spall rotates at the same speed as the rotor, i.e. $\phi_d = \omega_c dt + \phi_{do}$ (ϕ_{do}: initial starting location of the spall).

This model of the spall assumes that the rolling element will lose contact suddenly once it enters the spall region, and will regain contact instantly when exiting from that area (Figure-3.4.2 (a)). The abrupt change in the rolling element positions at the entry and exit of the spall results in very large impulsive forces in the system, which is not quite realistic. An modification on the previous model was introduced in [28] in which the depth of the fault (C_d) was modelled as a function of (ϕ_j), Figure-3.4.2 (b). The improvement on the model is to represent more realistic trajectory of the rolling element movement based on the relative size of the rolling element and the depth of the spall. Although, the profile of the trajectory appears much less abrupt than the earlier version; and apears to have only one position that may result in impulse, it still resulted in two impulses which does not agree with the experimental observation.

Careful observation of the interaction between the rolling element and spall leads to the trajectory is shown in Figure-3.4.3. The entry path of the rolling element has been represented as having a fixed radius of curvature (equal to that of the rolling element); entry of the rolling element in to the spall is therefore somewhat smoother. The smoother change in curvature at the entry would then represent a step in acceleration. On exiting the spall, the centre of the rolling element would have to change the direction suddenly, this representing a step change in velocity or an impulse in acceleration. This has been modelled as a sudden change (i.e. similar to the original model [28]). The resulting acceleration signal

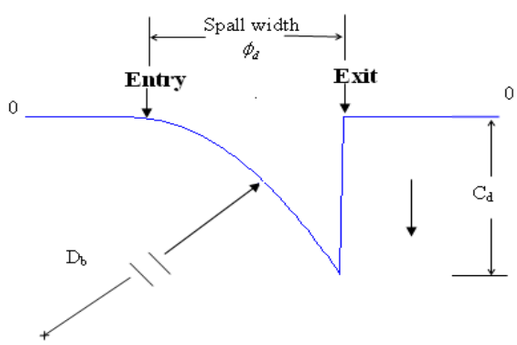

Fig. 3.4.3. A correlated model of a spall based on experimental data.

from this model appears to agree with the experimental observation, however author recommends further validation on this modelling approach and more updates are expected based on the findings.

For more detailed explanations on the modelling of REB fault refer to the works published by Sawalhi & Randall [29, 30, 31, 34, 35, 66, 67].

4. Conclusion

The techniques for modelling the effect of gearbox faults: tooth fillet cracks, tooth face spalls and bearing spalls, were presented and discussed in this chapter. The main purpose of the damage modelling is to simulate the effect of the faults on the dynamics of a geared transmission system that can be used in improving the understanding of the diagnostic information that manifest in the vibration signal mix from a gearbox.

The fault detection and diagnostic techniques based on vibration signal analysis are the ideal non-destructive machine health monitoring method, that can be applied in a minimally intrusive manner; i.e. by attaching an accelerometer on a gearbox casing. However, the dynamic interaction amongst the machine elements of a gearbox is often complex and the vibration signals measured from the gearbox is not easy to interpret. The diagnostic information that directly related to an emerging fault in a gear or a bearing is typically buried in the dominating signal components that are driven by the mechanisms of the transmission system themselves: For example, gear meshing signals.

Traditionally, the researchers worked on development of a signal processing technique for the gearbox diagnosis have embarked on their endeavours by making educated assumptions on the properties of the diagnostic information of the faults. These assumptions are often based on their careful observation of a measured vibration signals. However, the relevance of this approach is often somewhat limited by the simple fact that it's not easy to observe the key details of the fault signals from the signal mix.

It was demonstrated in this chapter how simulation models can be put to effective uses for studying the properties of the fault signals in greater details. A method of isolating the fault signals from the simulated gearbox signal mix was described in the section 3.3. The residual signals obtained from this process showed how the faults manifested in the resulting vibration signals in the "cleaned" state. The observation of the simulated residual signals has led to an improved understanding of the characteristics of impulses caused by the faults and the distorting effect of the transmission path (from the origin of the fault signal to the measurement location). The improved understanding of the fault signal obtained from the simulation studies led to the development of more effective signal processing techniques [34, 35, 62, 66].

The models of the gearbox faults presented in this work require further refinement. Some of the areas of future improvement aforementioned in the main body of the chapter include; improving the understanding of; the effect of plastic deformation in gear TFC, the effect of spall shapes and the effect of non-linear dynamic interaction of the gears and bearings. Improving the correlation between the simulated and the measured signals is a good way to demonstrate the understanding of the effect of faults in a geared transmission system. This

knowledge compliments the design and development efforts in vibration signal analysis based machine condition monitoring technologies. In the near future, accurately simulated signals of a faulty gearbox can aid the machine learning process of fault diagnosis algorithms based on neural networks. Performing this task in experiments are time consuming and costly exercise; simulation model based approach appears much more desirable.

The authors hope that the work presented in this chapter will stir the thoughts and the new ideas in readers that will contribute to the advancement of the gear engineering and the technologies in detecting and diagnosing the incipient faults in geared transmission systems.

5. Nomenclature

Unless otherwise stated the following tables defines the symbols and the acronyms used in this chapter.

$\overline{A_1A_2}$	A vector connecting points A_1 and A_2
Ø	Pressure Angle
LoA	Line of Action
PoA	Plane of Action
LoC	Line of Centres
R_b,, r_b	Gear Base Radius and Pinion Base Radius
R_{gear}, r_{pinion}	Gear Pitch Radius and Pinion Pitch Radius
R_o and r_o	Gear Outer Radius Pinion Outer Radius
P_b	Base pitch
CR	Contact Ratio
N	Number of teeth on a gear
TE	Transmission Error (Measured experimentally)
GTE	Geometrical Transmission Error
STE	Static Transmission Error
LTC	Long Term Composite of TE
STC	Short Term Composite of TE
ME	Motion Error (Numerically calculated TE)
x_i, y_i, z_i	Translation at i_{th} Degrees of Freedom
θ_{xi}, θ_{yi}, θ_{zi}	Rotation about a translational axis at i_{th} Degrees of Freedom
K, K_{mb}	Linear stiffness elements. The subscript 'mb' refers to stiffness at the gearmesh
C, C_{mb}	Damping matrices. The subscript 'mb' refers to damping at the gearmesh.
H	An 'on/off' switch governing the contact state of the meshing gear teeth.
$\underline{e_t}$	A vector representing the combined effect of tooth topography deviations and misalignment of the gear pair.
T	Torque

$\underline{x}$, $\underline{\dot{x}}$, $\underline{\ddot{x}}$	Vectors of displacement, velocity and acceleration (translation)
σ	Stress
ε	Strain

6. References

[1] J. D. Smith, and D. B. Welbourn, 2000, "Gearing Research in Cambridge", Cambridge Gearing Publications

[2] R. E. Smith, 1983, "Solving Gear Noise Problems with Single Flank Composite Inspection", The Gleason Works, Rochester, NY, USA

[3] R. G. Munro, D. Houser, 2004, "Transmission Error Concepts", Notes from Gear Noise Intensive Workshop, 19th ~ 21st July 2004, Melbourne, Australia

[4] R. W. Gregory, S. L. Harris and R. G. Munro, 1963a, "Dynamic Behaviour of Spur Gears", Proc IMechE, Vol. 178(1), pp 207-218

[5] R. W. Gregory, S. L. Harris and R. G. Munro, 1963b, "Torsional Motions of a Pair of Spur Gears", Proc IMechE Applied Mechanics Convention, Vol. 178 (3J), pp 166-173

[6] H. N. Ozguven and D. R. Houser, 1988a, "Mathematical Models Used in Gear Dynamics – A Review", Journal of Sound and Vibration, 121(3), pp 383-411

[7] C. C. Wang, 1985, "On Analytical Evaluation of Gear Dynamic Factors Based on Rigid Body Dynamics", Journal of Mechanism, Transmission and Automation in Design, Vol. 107, pp 301-311

[8] W. Bartelmus, 2001, "Mathematical Modelling and Computer Simulations as an Aid to Gearbox Diagnostics", Mechanical Systems and Signal Processing, 15 (5), pp 855-871

[9] J. Lin and R. G. Parker, 2002, "Mesh Stiffness Variation Instabilities in Two-Stage Gear Systems", Transaction of ASME, Jan 2002, Vol. 124, pp 68-76

[10] R. G. Parker and J. Lin, 2001, "Modelling, Modal Properties, and Mesh Stiffness Variation Instabilities of Planetary Gears", NASA, NASA/CR-2001-210939

[11] Y. Gao and R. B, Randall, 1999, "The Effect of Bearing and Gear Faults in Rolling Element Bearing Supported Gear Systems", DSTO Aeronautical and Maritime Research Laboratory, July 1999, CEVA-99-02

[12] Y. Gao and R. B. Randall, 2000, "Simulation of Geometric, Static and Dynamic Gear Transmission Errors", DSTO Aeronautical and Maritime Research Laboratory, Jan 2000, CEVA-2000-01

[13] M. Amabili, and A. Rivola, 1997, "Dynamic Analysis of Spur Gear Pairs: Steady-State Response and Stability of the SDOF Model with Time Varying Meshing Damping", Mechanical System and Signal Processing, 11 (3), pp 375-390

[14] I. Howard, S. Jia and J. Wang, 2001, "The Dynamic Modelling of a Spur Gear in Mesh Including Friction and A Crack", Mechanical Systems and Signal Processing, 15 (5), pp 831-853

[15] P. Velex and M. Maatar, 1996, "A Mathematical Model for Analysing the Influence of Shape Deviations and Mounting Error on Gear Dynamic Behaviour", Journal of Sound and Vibration, 191(5), pp 629-660

[16] S. M. Vijayakar, 1991, "A Combined Surface Integral and Finite Element Solution for a Three-Dimensional Contact Problem", International Journal of Numerical Methods in Engineering, 31, pp 524-546

[17] G. W. Blankenship and R. Singh, 1995, "A New Gear Mesh Interface Dynamic Model to Predict Multi-Dimensional Force Coupling and Excitation", Mechanical, Machine Theory, Vol. 30, No.1, pp43-57

[18] A. Kahraman and G. W. Blankenship, 1996, "Interactions between Commensurate parametric and Forcing Excitations in A System with Clearance", Journal of Sound and Vibration, 194 (3), pp 317-336

[19] R. G. Parker, 2000, "Non-Linear Dynamic Response of a Spur Gear Pair: Modelling and Experimental Comparisons", Journal of Sound and Vibration, 237(3), pp 435-455

[20] R. G. Parker, V. Agashe and S. M. Vijayakar, 2000, "Dynamic Response of a Planetary Gear System Using a Finite Element/Contact Mechanics Model", Transaction of ASME, Sep 2000, Vol. 122, pp 304-310

[21] CALYX, 2002, CALYX USER MANUAL, Advanced Numerical Solutions, Hilliard Ohio, U.S.A

[22] HELICAL, 2002, HELICAL 3D USER's MANUAL, Advanced Numerical Solutions, Hilliard Ohio, U.S.A

[23] S. Du, 1997, "Dynamic Modelling and Simulation of Gear Transmission Error for Gearbox Vibration Analysis", PhD dissertation, University of New South Wales

[24] N. S. Feng, E. J. Hahn, and R. B. Randall, 2002, "Using transient analysis software to simulate vibration signals due to rolling element bearing defects", Proceedings of the 3rd Australian congress on applied Mechanics, 689-694, Sydney.

[25] I. K. Epps and H. McCallion, 1994, "An investigation into the characteristics of vibration excited by discrete faults in rolling element bearings" (extract from PhD thesis of I.K. Epps), Annual Conference of the Vibration Association of New Zealand, Christchurch.

[26] D. Ho, 1999, "Bearing Diagnostics and Self Adaptive Noise Cancellation", PhD dissertation, UNSW.

[27] S. Fukata, E. H. Gad, T. Kondou, T. Ayabe and H. Tamura, 1985, "On the Vibration of Ball Bearings", Bulletin of JSME, 28 (239), pp. 899-904.

[28] A. Liew, N.S. Feng and E. J. Hahn, 2002, "Transient rolling element bearing systems", Trans. ASME Turbines and Power, 124(4), pp. 984-991

[29] N. Sawalhi and R.B. Randall, 2011, Vibration response of spalled rolling element bearings: observations, simulations and signal processing techniques to track the spall size. Mechanical Systems and Processing, 25 (3), (2011)

[30] N. Sawalhi and R.B. Randall, 2010, " Improved simulations for fault size estimation in rolling element bearings", paper presented at the seventh International Conference on Condition Monitoring and Machinery Failure Prevention Technologies, Stratford-upon-Avon, England, 22-24 June (2010).

[31] N. Sawalhi and R.B. Randall, 2008, "Localised fault diagnosis in rolling element bearings in gearboxes", paper presented at the Fifth International Conference on Condition Monitoring and Machinery Failure Prevention Technologies, Edinburgh, 15-18 July (2008).

[32] J. Sopanen & A Mikkola, 2003, "Dynamic model of a deep-groove ball bearing including localized and distributed defects. Prt 1: Theory", Proc of IMechE, vol. 217, Prt K, J of Multi-body Dynamics, 2003, pp 201-211.

[33] T. Tiwari, K. Gupta, O. Prakash, 2000, "Dynamic response of an unbalanced rotor supported on ball bearings", J of Sound & Vibration 238 (2000), pp757-779.

[34] N. Sawalhi & R. B. Randall, 2008, "Simulating gear and bearing interaction in the presence of faults: Prt II - Simulation of the vibrations produced by extended bearing faults", MSSP, Vol. 22, pp1952-1996 (2008).
[35] N. Sawalhi & R. B. Randall, 2008, "Simulating gear and bearing interaction in the presence of faults: Prt I - The combined gear bearing dynamic model and simulation of localized bearing faults", MSSP, Vol. 22, pp1924-1951 (2008).
[36] Z. -Q. Qu, 2004, "Model order reduction technique: with applications in Finite Element Analysis", Springer, 2004.
[37] R. Craig & M. Bumpton, 1968, "Coupling of substructures of dynamic analysis", AIAA Journal, 67 (1968), pp1313-1319.
[38] B. M. Irons, 1967, "Structural eigenvalue problem-elimination of unwanted variables", AIAA Journal, 3(5), pp961-962.
[39] L. Despnade, N.Sawalhi, R.B.Randall, "Improved Gearbox Simulations for Diagnostic and prognostics Purposes Using Finite Element Model Reduction Techniques", paper presented at the 6th Australasian Congress on Applied Mechanics, Perth, Australia, 12-15 December (2010
[40] C. Carmignani, P. Forte & G. Melani, 2009, "Component modal synthesis modelling of a gearbox fro vibration monitoring simulation", The 6th Int'l conf on Condition Monitoring Manhinery Failure Prevention Technology, Dublin, Ireland.
[41] N. Sawalhi, L. Deshpande and R. B. Randall, 2011, "Improved simulation of faults in gearboxes for diagnostic and prognostic purposes using a reduced finite element model of casing", AIAC 14 Fourteenth Australian International Aerospace Congress.
[42] R. Singh, 1989, "Analysis of Automotive Neutral Gear Rattle", Journal of Sound and Vibration, Vol. 131 (2), pp177-196
[43] A. Kahraman and R. Singh, 1991, "Interaction between Time-Varying Mesh Stiffness and Clearance Non-Linearity in Geared System", Journal of Sound and Vibration", 146, pp135-156
[44] D. P. Townsend, 1997, "Gear and Transmission Research at NASA", NASA-TM-107428
[45] A. K. Wong, 2001, "Vibration-Based Helicopter Health Monitoring – An Overview of the Research Program in DSTO", DSTO-HUMS2001
[46] L. E. Alban, 1985, "Systematic Analysis of Gear Failure", American Society of Metals, Metals Park OH, ISBN-0871702002
[47] G. DeLange, 1999, "Analyzing Gear Failures", Hydrocarbon Processing, Features: 4/00, www.hydrocarbonprocessing.com
[48] DANA, 2002, Raodranger, "Understanding Spur Gear Life", EATON and DANA Corporation, TRSM-0913, (www.roadranger.com)
[49] ANSI/AGMA, 1995, "Appearance of Gear Teeth – Terminology of Wear and Failure", American Gear Manufacturers Association, ANSI/AGMA 1010-E95
[50] HyGears, HyGears © V2.0 Gear Design and Analysis Software, Involute Simulation Software Inc
[51] D. G. Lewicki, 2001, "Gear Crack Propagation Path Studies – Guidelines for Ultra-Safe Design", NASA-TM- 2001 211073
[52] T. J. Curtin, R. A. Adey, J. M. W. Bayman and P. Marais, 1998, Computational Mechanics Inc, Billerica, Massachusetts, 01821, USA

[53] D. G. Lewicki, 1998, “Three-Dimensional Gear Crack Propagation Studies”, NASA-TM-1998-208827

[54] S. Pehan, T. K. Hellen, J. Flasker and S. Glodes, 1997, “Numerical Methods for Determining Stress Intensity Factors VS Crack Depth in Gear Tooth Roots”, Int J of Fatigue, Vol. 19, No. 10, pp677-685

[55] M. Guagliano and L. Vergani, 2001, “Effect of Crack Closure on Gear Crack Propagation”, Int J or Fatigue, Vol. 23, pp67-73

[56] H. Endo, C. Gosselin, R. B. Randall, (Sept 2004), “The effects of localized gear tooth damage on the gear dynamics – A comparison of the effect of a gear tooth root crack and a spall on the gear transmission error”, IMechE, 8th International Conference on Vibrations in Rotating Machinery, University of Wales, Swansea

[57] W. D. Mark, C. P. Reagor and D. R. McPherson, 2007, "Assessing the role of plastic deformation in gear-health monitoring by precision measurement of failed gears", MSSP, 21: pp177-192 (2007)

[58] T. E. Tallian, 1992, “Failure Atlas fir Hertz Contact Machine Elements”, ASME Press, ISBN 0-7918-0008-3

[59] Y. Ding and N. F. Rieger, 2003, “Spalling formation Mechanism for Gears”, Wear, 254 2003), pp1307-1317

[60] W. D. Mark and C. P. Reagor, 2007, "Static transmission error vibratory excitation contribution from plastically deformed gear teeth caused by tooth bending fatigue damage", MSSP, 21: pp885-905 (2007)

[61] H. Endo, R. B. Randall and C. Gosselin, 2004, “Differential Diagnosis of Spall vs. Cracks in the Gear Tooth Fillet Region”, Journal of Failure Analysis and Prevention, Vol4, Issue 5, Oct 2004

[62] H. Endo, R. B. Randall and C. Gosselin, 2008, “Differential Diagnosis of Spall vs. Cracks in the Gear Tooth Fillet region: Experimental Validation”, Journal of Mechanical System and Signal Processing, due to be published on 19/Jan/2009, Vol23 Issue3.

[63] M. EL Badaoui, J. Antoni, F. Guillet and J. Daniere, 2001a, “Use of the Moving Cepstrum Integral to Detect and Localise Tooth Spalls in Gears”, Mechanical System and Signal Processing, 2001, 15 (5) , 873-885

[64] M. EL Badaoui, V. Cahouet, F. Guillet, J. Daniere and P. Velex, 2001b, “Modelling and Detection of Localized Tooth Defects in Geared Systems”, Transaction of ASME, Sep, 2001, Vol. 123, pp422-430

[65] J. Mahfoudh, C. Bard, M. Alattass and D. Play, 1995, “Simulation of Gearbox Dynamic Behaviour with Gear Faults”, I Mech E, C492/045/95

[66] N.Sawalhi, R.B.Randall and H.Endo, “Gear and bearing fault simulation applied to diagnostics and prognostics”, paper presented at The 19th International Congress and Exhibition on Condition Monitoring and Diagnostic Engineering Management, Luleå, Sweden, June (2006).

[67] N. Sawalhi, and R.B. Randall, Vibration response of spalled rolling element bearings: observations, simulations and signal processing techniques to track the spall size. Mechanical Systems and Processing, 25 (3), (2011).

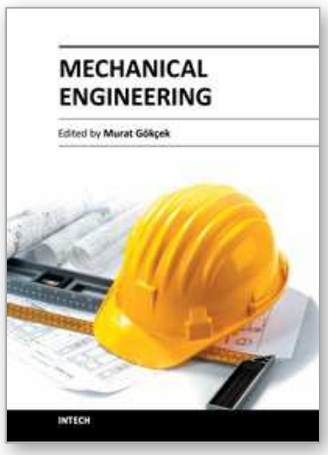

Mechanical Engineering

Edited by Dr. Murat Gokcek

ISBN 978-953-51-0505-3
Hard cover, 670 pages
Publisher InTech
Published online 11, April, 2012
Published in print edition April, 2012

The book substantially offers the latest progresses about the important topics of the "Mechanical Engineering" to readers. It includes twenty-eight excellent studies prepared using state-of-art methodologies by professional researchers from different countries. The sections in the book comprise of the following titles: power transmission system, manufacturing processes and system analysis, thermo-fluid systems, simulations and computer applications, and new approaches in mechanical engineering education and organization systems.

How to reference

In order to correctly reference this scholarly work, feel free to copy and paste the following:

Endo Hiroaki and Sawalhi Nader (2012). Gearbox Simulation Models with Gear and Bearing Faults, Mechanical Engineering, Dr. Murat Gokcek (Ed.), ISBN: 978-953-51-0505-3, InTech, Available from: http://www.intechopen.com/books/mechanical-engineering/gearbox-simulation-models-with-gear-and-bearings-faults

INTECH
open science | open minds

InTech Europe
University Campus STeP Ri
Slavka Krautzeka 83/A
51000 Rijeka, Croatia
Phone: +385 (51) 770 447
Fax: +385 (51) 686 166
www.intechopen.com

InTech China
Unit 405, Office Block, Hotel Equatorial Shanghai
No.65, Yan An Road (West), Shanghai, 200040, China
中国上海市延安西路65号上海国际贵都大饭店办公楼405单元
Phone: +86-21-62489820
Fax: +86-21-62489821

IntechOpen